Please fill in the name of the event you are preparing this manuscript for.	SPE Virtual Improved Oil Recovery Conference IOR2022
Please fill in your 6-digit SPE manuscript number.	SPE-209380-MS
Please fill in your manuscript title.	Reaction kinetics determined from core flooding and steady state principles for Stevns Klint and Kansas chalk injected with MgCl2 brine at reservoir temperature

Please fill in your author name(s) and company affiliation.

Given Name	Middle Name	Surname	Company
Pål	Østebø	Andersen	Department of Energy Resources, University of Stavanger, 4021 Norway
Reidar	Inge	Korsnes	Department of Energy and Petroleum Engineering, University of Stavanger, 4021 Norway
Andre	Tvedt	Olsen	Department of Energy Resources, University of Stavanger, 4021 Norway
Erik		Bukkholm	Department of Energy Resources, University of Stavanger, 4021 Norway

Abstract

A methodology is presented for determining reaction kinetics from core flooding: A core is flooded with reactive brine at different compositions with injection rates varied systematically. Each combination is performed until steady state, when effluent concentrations no longer change significantly with time. Lower injection rate gives the brine more time to react. We also propose shut-in tests where brine reacts statically with the core a defined period and then is flushed out. The residence time and produced brine composition is compared with the flooding experiments. This design allows characterization of the reaction kinetics from a single core. Efficient modeling and matching of the experiments can be performed as the steady state data are directly comparable to equilibrating the injected brine gradually with time and does not require spatial and temporal modeling of the entire dynamic experiments. Each steady state data point represents different information that helps constrain parameter selection. The reaction kinetics can predict

equilibrium states and time needed to reach equilibrium. Accounting for dispersion increases the complexity by needing to find a spatial distribution of coupled solutions and is recommended as a second step when a first estimate of the kinetics has been obtained. It is still much more efficient than simulating the full dynamic experiment.

Experiments were performed injecting 0.0445 and 0.219 mol/L $MgCl_2$ into Stevns Klint (Denmark) and Kansas (USA) chalks at 100 and 130°C (North Sea reservoir temperature). Injection rates were varied from 0.25 to 16 PV/d while shut-in tests provided equivalent rates down to 1/28 PV/d. The results showed that Ca^{2+} ions were produced and Mg^{2+} ions retained (associated with calcite dissolution and magnesite precipitation, respectively). This occurred in a substitution-like manner, where the gain of Ca was similar to the loss of Mg^{2+}. A simple reaction kinetic model based on this substitution with three independent tuning parameters (rate coefficient, reaction order and equilibrium constant) was implemented together with advection to analytically calculate steady state effluent concentrations when injected composition, injection rate and reaction kinetic parameters were stated. By tuning reaction kinetic parameters, the experimental steady state data were fitted efficiently. The parameters were determined relatively accurate for each core. The roles of reaction parameters, pore velocity and dispersion were illustrated with sensitivity analyses. The determined reaction kinetics could successfully predict the chemical interaction in reservoir chalk and outcrop chalk containing oil with strongly water-wet or mixed-wet state.

The steady state method allows computationally efficient matching even with complex reaction kinetics. Using a comprehensive geochemical description in the software PHREEQC, the kinetics of calcite and magnesite mineral reactions were determined by matching the steady state concentration changes as function of (residence) time. The simulator predicted close to identical production of Ca as loss of Mg. The geochemical software predicted much higher calcite solubility in $MgCl_2$ than observed at 100 and 130°C for Stevns Klint and Kansas. The methodology supports reactive flow modeling in general, but especially oil-bearing chalk reservoirs which are chemically sensitive to injected seawater in terms of wettability and rock strength.

Keywords: Reaction kinetics; Chalk; Steady state; Core flooding experiments; Analytical solutions

1. Introduction

In this work we are interested in determining reaction kinetics from single phase core flooding with reactive brines, with focus on chalk. Chalk is a biogenic porous rock composed of calcareous microfossils, with high porosity (~40%) and low permeability (1-5 mD) (Hjuler and Fabricius 2009; Andersen et al. 2018; Kallesten et al. 2021b). Water-rock chemical reactions have many implications such as altering wettability, geomechanical strength and porosity-permeability relations which are important for geological storage of CO_2, production of hydrocarbons, seabed subsidence and aquifer remediation (Maury et al. 1996; Sylte et al. 1999; Heggheim et al. 2005; Puntervold and Austad 2008; Lebedev et al. 2017; Kallesten et al. 2020; Sabo and Beckingham 2021; Bonto et al. 2021). Seawater-like brines containing divalent ions such as Ca^{2+}, Mg^{2+} and SO_4^{2-} have demonstrated reactivity towards chalk at high temperature, especially in the range of Norwegian Continental Shelf reservoirs Valhall and Ekofisk with 92 and 130°C, respectively (Megawati et al. 2013; Minde et al. 2018). In oil-water systems, adsorption of these ions can cause detachment of negatively charged oil components (Zhang et al. 2006). They can also trigger dissolution of calcite and precipitation of minerals such as magnesite and anhydrite (Madland et al. 2011). Sulfate adsorption and calcite dissolution have been linked to weakening of the chalk matrix in terms of bulk modulus, yield strength and creep strain profiles of outcrop chalks (Korsnes et al. 2008; Megawati et al. 2011, 2013; Andersen et al. 2018; Minde et al. 2018). Other proposed weakening

mechanisms include pressure solution (Hellmann et al. 2002). Chemical weakening has been demonstrated for Eldfisk (Kallesten et al. 2021a) and Dan field reservoir chalk (Amour et al. 2021).

Simulation of reactive flow in porous media is typically done with advection-dispersion-reaction equations (Appelo and Postma 2005; Berkowitz et al. 2016; Steefel and MacQuarrie 2018). Earlier works modeling reactive flow in chalk (Evje et al. 2009; Andersen et al. 2012) have combined effluent data from several core flooding tests, each using a single test condition, but uncertainty can arise from core-to-core variation. It is also possible to apply information on mineralogical changes from a flooding test to characterize the reaction kinetics (Andersen et al. 2018), but this relies on expensive techniques and that the mineralogical changes are sufficient for accurate quantification. Andersen and Berawala (2019) interpreted a vast set of experimental data to both determine reaction kinetics and the associated impact on creep compaction for Aalborg (Denmark) and Liege (Belgium) chalks. Kallesten et al. (2020) extended this methodology to account for flow in compacting fractured chalk with permeability alterations in the matrix and fracture.

In this work we present a methodology to interpret reactive flow experiments. The main principle is to focus on the steady state data collected when effluent concentrations do not change further with time for given injected composition, injection rate, core properties, temperature and pressure. Such measurements depend only on the dynamic equilibrium between reactions, advection and to some extent dispersion, while transient events and mechanisms (adsorption, etc) can be ignored. This is also demonstrated mathematically later in the paper. By measuring such data under different injected compositions, injected rates and temperatures we hypothesize that we are able to characterize the reaction kinetics in great detail. This is demonstrated by performing reactive flow experiments on chalk cores at varied conditions with the purpose of collecting steady state data. A key advantage from the interpretation perspective is that complicated reactive transport equations can be simplified by ignoring the changes in time and only simulating and matching the steady state. As exemplified in previous studies (Evje et al. 2009; Andersen et al. 2012, 2018), the impact of mineralogical reactions gives a fixed outlet concentration profile at steady state which, as will be shown here, does not require transient simulations to match. Steady state principles in multiphase flow core flooding have also been used in the context of relative permeability measurements where the dynamic equilibrium between advective and capillary forces have allowed more accurate estimation of relative permeabilities and even estimation of capillary pressure (Virnovsky et al. 1995; Andersen et al. 2020; Andersen 2021).

The paper is structured as follows: The experimental setup is presented in **Section 2** with fluids, rock material and the tested conditions. General equations describing advection-reaction-dispersion systems are listed in **Section 3** and then formulated under steady state assumptions. Adapted descriptions to our experimental setting are provided in **Section 4**, also allowing analytical solutions for a specific choice of model assumptions. Results are shown in **Section 5** where we use the analytical solution to interpret the data with accurate estimation of limited tuning parameters. Sensitivity analyses are performed to illustrate the solution and the advection-reaction interplay. We also demonstrate matching of the experimental data with a comprehensive geochemistry description using a geochemical simulator. The paper is summarized with conclusions in **Section 6**.

2. Experimental setup

2.1. Rock material and fluids

Outcrop chalk from two locations were used in this study: (1) Stevns Klint (Denmark) chalk from the Tor Formation, in particular the Sigerslev Member, of middle Upper Maastrichtian age (Surlyk et al. 2006) and (2) Kansas (USA) chalk from the Niabrara Formation, from the lowermost Fort Hayes Member which is of Early Coniacian age (Da Gama et al. 2014). Stevns Klint is a very pure chalk with >99 weight percent (wt%) calcite and specific surface area of ~2 m^2/g while Kansas chalk is less pure with a calcite content

between 95-97 wt% and specific surface area of ~3 m^2/g (Andersen et al. 2018). The non-carbonate in Kansas chalk is quartz and phyllosilicate clays, while in Stevns Klint traces were found of quartz, smectite and illite (Andersen et al. 2018). In comparison, reservoir chalk was found to have higher impurity with quartz content around 10-15 wt% and presence of clays (Kallesten et al. 2021b). Test samples were made from cylindrical shaped cores drilled from chalk blocks. The cores were shaped to a diameter of 38.1 mm by the use of a turning lathe and cut to a length of approximately 70 mm. This is a standard size used in our laboratory. In total three Stevns Klint (SKA) cores and one Kansas (KR) core were flooded in this study, see **Table 1**.

Table 1 Core identification, test temperature, injection brine and porosity.

Core ID	Temperature [°C]	Injection brine	Length [mm]	Diameter [mm]	Dry mass [g]	Saturated mass [g]	1 PV/day [mL/min]	Porosity [%]
SKA1	130	0.219 M $MgCl_2$	73.83	38.05	119.28	159.07	0.028	47.4
SKA2	130	0.219 M $MgCl_2$ and 0.0445 M $MgCl_2$	69.69	38.04	109.85	148.33	0.027	48.5
SKA3	100	0.219 M $MgCl_2$	71.25	38.03	119.45	156.22	0.026	45.4
KR30	130	0.219 M $MgCl_2$	74.46	38.05	141.23	173.79	0.023	38.5

Two $MgCl_2$ brines were used, 0.219 M -and 0.0445 M $MgCl_2$. These brines were prepared by adding $MgCl_2$ x $6H_2O$ to $CaCO_3$ equilibrium water. The cores SKA1, SKA3 and KR30 were flooded with 0.219 M $MgCl_2$ during their entire test sequence. SKA2 had a 21 day shut-in period and a 14 day injection period, both with 0.219 M $MgCl_2$ before the injected brine was changed to 0.0445 M $MgCl_2$ for the remaining part of the test. The part of this test with high concentration was performed to check whether the chemical response of this core was the same as other cores under same conditions. To evaluate the role of temperature on reaction kinetics, SKA3 was tested at 100 °C, while the three other cores were tested at 130 °C. Detailed test schedules, conditions and corresponding concentration measurements are listed in **Appendix A** in **Table 4** (SKA1), **Table 5** (SKA2), **Table 6** (SKA3) and **Table 7** (KR30).

2.2. Flooding procedure

Reactive flow experiments were performed in triaxial cells, **Figure 1**, with the capability to run tests at reservoir temperatures and stresses, measure axial and radial deformation and permeability. Core compaction may reduce the pore volume and residence time, but also generate new surface area when grains are broken. Since the main objective of this study is brine-rock interactions, the experiments were performed at low effective stresses to obtain limited core deformations. Confining pressure was set to 2 MPa for all tests, except the core KR30 where it was 1.2 MPa. The pore pressure was 0.7 MPa to avoid boiling at temperatures above 100 °C. Tests were performed at 100 °C and 130 °C with an initial flow rate of one pore volume per day (PV/day) for all tests. During the experimental test sequences, the flow rates varied from 0.25 PV/day to 16 PV/day. During brine injection, effluent samples were collected at regular intervals and analyzed using a Dionex ICS 5000 ion chromatograph. Flow rates were changed mainly when effluent concentrations reached steady state values, but in some cases the rates were changed earlier in the interest of time and when the expected change in concentrations of the long term trend was small compared to the change already observed.

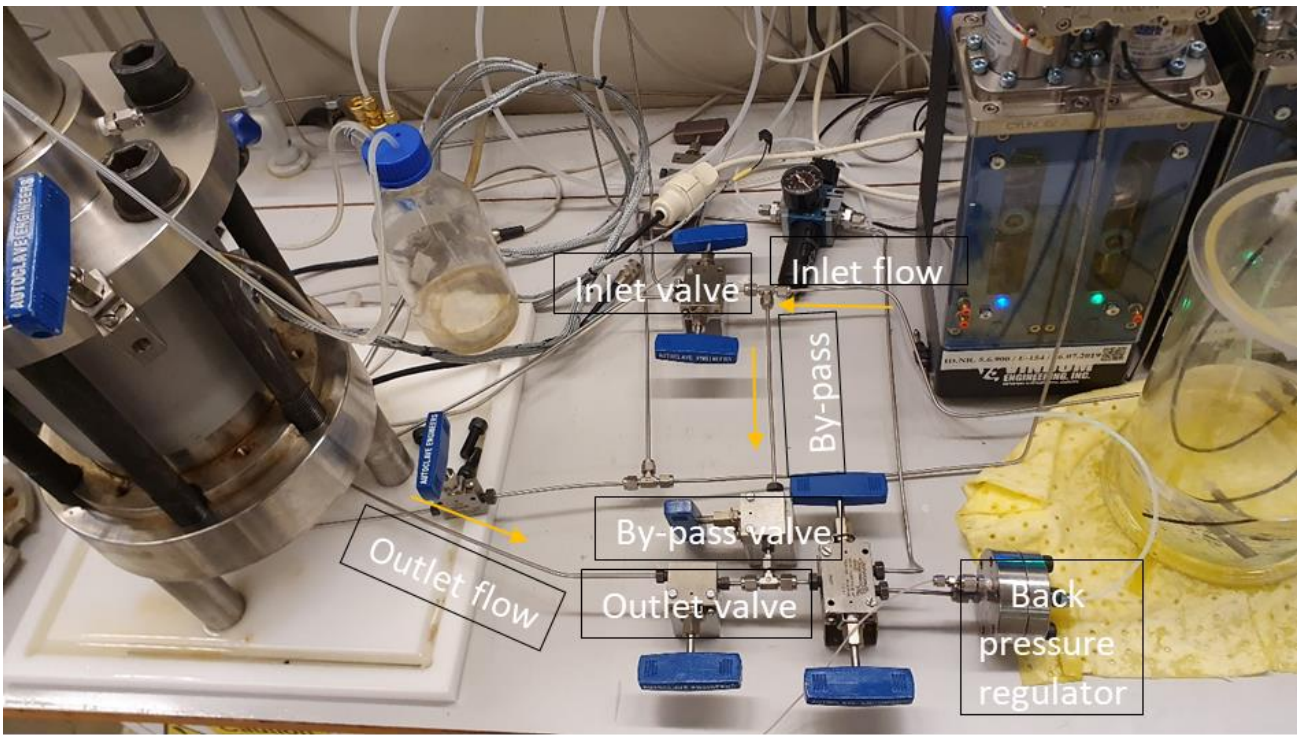

Figure 1 The experimental setup with triaxial cell to the left, pump on the right side and various valves and flow lines indicated.

2.3. Shut in procedure

Shut-in tests set to last from one day to 28 days were performed for all cores. Due to the setup of the triaxial cell injection system, a complete shut-in of the cores was not possible. In the present setup, valves at the inlet and outlet side of the core, **Figure 1**, could be closed and thereby making it a complete shut-in system. But closing both valves would prevent the pore pressure to be measured inside the core. Any leakages inside the closed system would lead to pore pressure loss that could hamper the experiment. To have control over the pore pressure, it was decided to close the inlet injection valve, open a by-pass valve such that brine could by-pass the triaxial cell and flow directly towards the back pressure regulator. The outlet valve from the triaxial cell would remain open thereby securing constant pore pressure inside the core. This set-up prevents new brine to be injected into the core, but with the outlet valve open, ions in the brine will have the possibility to diffuse in or out of the core. Diffusion is slow in porous media and assumed to have limited effect (mainly near the open boundary). The stored brine is expected to have a uniform concentration profile after shut-in (same reaction time at every location), reflected in the produced fluid after shut-in. Deviation from the stable level in the first produced fluid could indicate diffusive interaction.

3. Theory

3.1. General description of advection-dispersion-reaction systems

Reactive flow in a 1D porous medium representing the core plug is considered where the cross-sectional area and porosity are assumed uniform and constant. See **Figure 2** for an illustration of the system and two of the core plugs (after the experiment).

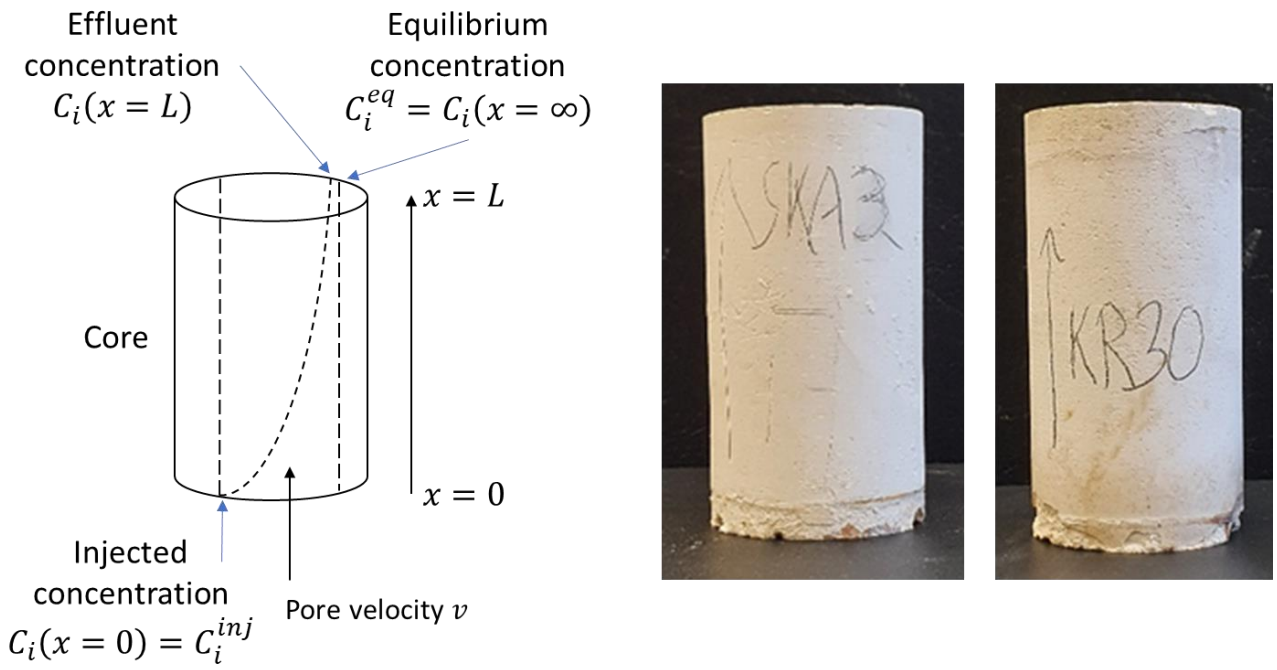

Figure 2 Left: An illustration of the system. A core is flooded with brine having an injected composition C_i^{inj} and the brine flows with pore velocity v. Reactions alter the brine to its outlet composition $C_i(x = L)$. If the brine interacts long enough it reaches its equilibrium composition C_i^{eq}. This is indicated as the greatest possible change in concentration from the injected composition. Right: Two of the cores (SKA3 and KR30) after the experiments. The flow direction is indicated on the cores with arrows.

General equations describing transport of reactive ions are given as (Appelo and Postma 2005; Lichtner et al. 2018):

$$\partial_t(C_i + \rho_i^s) = -v\partial_x C_i + D\partial_{xx} C_i + \dot{r}_i(a_1, \dots, a_{N_{ions}}), \qquad (i = 1{:}\, N_{ions}) \tag{1}$$

C_i represents the molar concentration (mol per m3) in the brine, ρ_i^s the concentration of adsorbed species (also in mol per pore volume), v is the pore velocity of the brine (volumetric rate per porous cross section), D is the dispersion coefficient and $\dot{r}_i$ is a source term of the species related to mineralogical reactions. N_{ions} is the number of ions. Also, we have equations for N_{min} mineral species with concentrations ρ_j (in mol per unit pore volume):

$$\partial_t \rho_j = \dot{r}_j(a_1, \dots, a_{N_{ions}}), \qquad (j = 1{:}\, N_{min}) \tag{2}$$

Mineralogical reaction rates and their equilibria depend on aqueous species activities a_i, defined based on activity coefficients γ_i and molalities of free species (here we assume molar concentrations and molalities are the same) (Lasaga 1998).

$$a_i = \gamma_i m_i, \qquad (i = 1{:}\, N_{ions}) \tag{3}$$

m_i is then the concentration of free species i. The remaining part of the total concentration C_i is bound in aqueous complexes with concentrations $n_{i,i'}$, formed between different components i' in the brine. The formation of a complex AB between species A and B can be described by the dissociation reaction and equilibrium equation:

$$\mathrm{AB} \rightleftharpoons \mathrm{A} + \mathrm{B}, \qquad K_{\mathrm{AB}} = \frac{a_{\mathrm{A}} a_{\mathrm{B}}}{a_{\mathrm{AB}}}, \tag{4}$$

for an equilibrium constant K_{AB}, where the activities are described by (3). The total concentration of a dissolved species is divided into its free ion concentration m_i and complex concentrations $n_{i,i'}$:

(5) $$C_i = m_i + \sum_{i':comp} n_{i,i'}.$$

Activity coefficients and complexation can both affect the dissolution and precipitation reactions of minerals, since it is the activity of free species that determine their rate and equilibria. For treatment of surface species, which are less relevant in this work, we refer to Appelo and Postma (2005). The activity coefficients are primarily a function of ionic strength, ionic valence z_i and temperature T. Ionic strength I_0 is defined by:

(6) $$I_0 = \frac{1}{2}\sum_i m_i z_i^2 + \frac{1}{2}\sum_{i,i'} n_{i,i'} z_{i,i'}^2,$$

The activity coefficients can be defined by the Truesdell-Jones equation (Appelo and Postma 2005), which is valid for high ionic strength brines:

(7) $$\log \gamma_i = -\frac{A(T) z_i^2 \sqrt{I_0}}{1 + \tilde{a}_i B(T)\sqrt{I_0}} + \tilde{b}_i I_0,$$

$A(T), B(T)$ are temperature functions and $\tilde{a}_i, \tilde{b}_i$ are ion specific parameters. In addition, there will be charge balance given by:

(8) $$\sum_i m_i z_i + \sum_{ij} n_{ij} z_{ij} = 0$$

The boundary conditions we consider are a fixed injected composition C_i^{inj} at the inlet (pore velocity v) while the flow passes the outlet at $x = L$ without interaction, as in a semi-infinite system. An initial composition C_i^{init} can be defined (but will not be relevant when considering steady state).

(9) $$C_i(x = 0) = C_i^{inj}, \qquad C_i(t = 0) = C_i^{init}$$

3.2. Steady state in an advection-dispersion-reaction system

We define steady state as when the ionic concentrations no longer change with time. In typical surface complexation or ion exchange models the surface species concentrations are a function of the brine composition, and at steady state they can therefore be considered constant as well. The time derivative in (1) can therefore be set to zero. We scale the spatial axis by the core length $X = \frac{x}{L}$ and obtain:

(10) $$d_X C_i = \frac{D}{vL} d_{XX} C_i + \frac{L}{v}\dot{r}_i(a_1, \dots, a_{N_{ions}}), \qquad (i = 1{:}\, N_{ions})$$

Assume the grid consists of N_x cells such that X_k denotes the scaled distance from the inlet boundary to the grid cell centers. We have $X_{1/2} = 0$ and $X_{N_m+1/2} = 1$. For simplicity assume uniform discretization: $\Delta X = 1/N_x$ and discretize the central cells around point :

(11) $$\frac{[C_i]_k - [C_i]_{k-1}}{\Delta X} = \frac{D}{vL\Delta X}\left[\frac{[C_i]_{k+1} - [C_i]_k}{\Delta X} - \frac{[C_i]_k - [C_i]_{k-1}}{\Delta X}\right] + \frac{L}{v}[\dot{r}_i]_k, \qquad (k = 2{:}\, N_x - 1)$$

The inlet boundary is represented by a constant injected concentration $[C_i]_0 = C_i^{inj}$ in a ghost cell at $k = 0$:

(12) $$\frac{[C_i]_k - C_i^{inj}}{\Delta X} = \frac{D}{vL\Delta X}\left[\frac{[C_i]_{k+1} - [C_i]_k}{\Delta X} - \frac{[C_i]_k - C_i^{inj}}{\Delta X}\right] + \frac{L}{v}[\dot{r}_i]_k, \qquad (k = 1)$$

Dispersion at the inlet is included with the above formulation, but can be ignored by setting the inlet dispersion flux to zero. In the last cell the dispersion flux is set to zero:

$$\frac{[C_i]_k - [C_i]_{k-1}}{\Delta X} = \frac{D}{vL\Delta X}\left[0 - \frac{[C_i]_k - [C_i]_{k-1}}{\Delta X}\right] + \frac{L}{v}[\dot{r}_i]_k, \qquad (k = N_x) \tag{13}$$

Assuming zero dispersive flux at a boundary corresponds to letting the component transport there be only due to bulk movement of water. The N_x equations above for each of the N_{ions} ions are nonlinear and dependent and must be solved simultaneously. In addition, equations for complex equilibria, mass balance, charge balance, ionic strength and activity coefficients must be solved in each cell. This is performed by linearizing the involved equations and solving the resulting linear system iteratively until the nonlinear equations are solved.

3.3. Steady state in an advection-reaction system

Next, we consider the special case of ignoring dispersion, by setting $D = 0$. This is often assumed when interpreting experimental data, as advection and reactions are believed to be the dominant mechanisms. Then (10) simplifies to:

$$d_X C_i = \frac{L}{v}\dot{r}_i, \qquad (i = 1{:}\, N_{ions}) \tag{14}$$

and its discretized version:

$$\frac{[C_i]_k - [C_i]_{k-1}}{\Delta X} = \frac{L}{v}[\dot{r}_i]_k, \qquad [C_i]_0 = C_i^{inj}, \qquad (k = 1{:}\, N_x) \tag{15}$$

Note that the solution in cell k can be calculated directly once the solution in cell $k-1$ is known, thus making a much simpler system to solve. We can also note that by integrating (14), the change in composition from the inlet to a position X is exactly equal to the impact of letting the injected brine equilibrate with the rock with reaction time equal to the time it has traveled through the system:

$$\Delta C_i = \int_{X=0}^{X} \frac{L}{v}\dot{r}_i dX = \int_{t=0}^{t} \dot{r}_i dt\,, \qquad (i = 1{:}\, N_{ions}) \tag{16}$$

Again, the N_{ions} transport equations are coupled as the reaction rates can depend simultaneously on all the involved ions. They also depend on equilibrium constraints, mass balances, charge balance, activity coefficients, etc., local to the given cell and must be solved too.

3.4. Shut-in procedure and matching

An important implication of (16) is that when dispersion is ignored, the change in composition due to transporting injected brine through the core a given time, is the same as letting the brine react with rock that same amount of time. We can therefore saturate the core with injected composition, store it without flooding for a specified shut-in period τ [d] to let reactions happen, and then quickly flood out the brine to test its composition. The equivalent injection rate (to give the same residence time) is then $1/\tau$ [PV/d]. This method allows us to obtain measurements at low equivalent rates.

It also demonstrates that simulation of steady state experiments is directly comparable to the gradual equilibration of injected brine, which can be evaluated in one cell instead of an entire grid representing the core. By drawing the composition as function of time we can directly compare with effluent compositions with different residence times (the time taken to travel through the core).

4. Theoretical description of the $MgCl_2$-calcite system

4.1. Detailed description

Before proceeding it is useful to describe in more detail the specific system we are testing experimentally. During $MgCl_2$ brine injection into clean chalk, the main aqueous species include calcium Ca, magnesium Mg and carbon C, which are reactive, and Cl, which is inert. The main minerals include calcite $CaCO_3$ (*c*), the primary constituent of chalk, but also magnesite $MgCO_3$ (*m*) which forms by precipitation from the reactive brine (Madland et al. 2011; Andersen et al. 2018). Other minerals, either preexisting or formed are assumed to be of less importance. The mineral reactions can be given as:

$$\text{(17)} \qquad CaCO_3(s) + H^+ \leftrightarrow Ca^{2+} + HCO_3^-, \qquad MgCO_3(s) + H^+ \leftrightarrow Mg^{2+} + HCO_3^-,$$

Each of them is described by a reaction rate. Equilibrium reactions for aqueous carbon species and water dissociation are given by:

$$\text{(18)} \qquad CO_2(aq) + H_2O \leftrightarrow HCO_3^- + H^+, \qquad HCO_3^- \leftrightarrow CO_3^{2-} + H^+, \qquad H_2O \leftrightarrow OH^- + H^+,$$

Some relevant aqueous complexes in the system and their reactions are given by:

$$\text{(19)} \qquad CaCl^+ \leftrightarrow Ca^{2+} + Cl^-, \qquad MgCl^+ \leftrightarrow Mg^{2+} + Cl^-$$

The total concentrations of aqueous species we keep track of are for calcium, magnesium, chloride and carbon: $C_{Ca}, C_{Mg}, C_C, C_{Cl}$. The mineral species concentrations are ρ_c, ρ_m. These six concentrations are described by the conservation laws below (surface species are ignored):

$$\text{(20)} \qquad \partial_t C_{Ca} = -v\partial_x C_{Ca} + D\partial_{xx} C_{Ca} + \dot{r}_{Ca},$$

$$\text{(21)} \qquad \partial_t C_{Mg} = -v\partial_x C_{Mg} + D\partial_{xx} C_{Mg} + \dot{r}_{Mg},$$

$$\text{(22)} \qquad \partial_t C_C = -v\partial_x C_C + D\partial_{xx} C_C + \dot{r}_C,$$

$$\text{(23)} \qquad \partial_t C_{Cl} = -v\partial_x C_{Cl} + D\partial_{xx} C_{Cl} + \dot{r}_{Cl},$$

$$\text{(24)} \qquad \partial_t \rho_c = \dot{r}_c,$$

$$\text{(25)} \qquad \partial_t \rho_m = \dot{r}_m.$$

To calculate the 8 free ion concentrations $m_{Ca}, m_{Mg}, m_{Cl}, m_{CO2}, m_{HCO3}, m_{CO3}, m_H, m_{OH}$ and 2 complex concentrations n_{CaCl}, n_{MgCl} locally we apply 5 equilibrium equations for the 5 equilibrium reactions in (18) and (19), 1 charge balance (8), 3 mass balances (5) for how the species Ca, Mg, Cl are divided into free species and the 2 complexes and 1 mass balance for the carbon species (26):

$$\text{(26)} \qquad C_C = m_{HCO3} + m_{CO3} + m_{CO2}.$$

As the activities determine the equilibria and reaction rates; 1 ionic strength for the brine and 10 activity coefficients for the brine species must be calculated using the 11 equations (6) and (7). Summarized we obtain 6 conservation equations and 21 constraint equations solved for 27 unknowns in one cell, where the conservation laws in a cell also are coupled with the unknowns in the two neighboring cells.

This system can be modeled using a geochemical software, in this work PHREEQC v3.6.2 (Parkhurst and Appelo 1999). We apply the LLNL database which includes species, their activity coefficients, equilibrium reactions and their equilibrium constants and finally dissolution constants for minerals at the relevant temperatures. The database also includes more complexes (combinations of aqueous species), but the most relevant species that affect the reaction kinetics are described above. The equilibrium constants are assumed known, while the reaction rates for calcite and magnesite are determined by matching experimental data. Their rates are assumed to be of the form (Lasaga 1998; Morse and Arvidson 2002):

$$\dot{r}_c = -k_c\left(1-\Omega_c^{n_c}\right),\ \ \dot{r}_m = -k_m\left(1-\Omega_m^{n_m}\right),\ \ \Omega_c = \frac{a_{HCO3}a_{Ca}}{K_c a_H},\ \ \Omega_m = \frac{a_{HCO3}a_{Mg}}{K_m a_H} \tag{27}$$

Ω_c, Ω_m denote the saturation states of calcite and magnesite, respectively, and yield precipitation of the given mineral when above 1, and dissolution when less than 1. A value equal to 1 means the mineral is in equilibrium. K_c, K_m are the solubility products. The coefficients k_c, k_m and exponents n_c, n_m are treated as the only 4 tuning parameters. Ignoring dispersion, all other parameters are known from the database or the experimental conditions. We note that the source terms of the aqueous species are related by reaction stoichiometry to the mineral terms as:

$$\dot{r}_{Ca} = -\dot{r}_c, \qquad \dot{r}_{Mg} = -\dot{r}_m, \qquad \dot{r}_C = -\dot{r}_m - \dot{r}_c, \qquad \dot{r}_{Cl} = 0. \tag{28}$$

Running dynamic geochemical simulations are time consuming, especially if many interactions between brine and surroundings are considered such as mineral precipitation or dissolution, ion exchange and dispersion. With more minerals and aqueous species, high reaction rates, fine grid, short time steps and long durations it may be even impractical to run the simulations. Considering that we wish to history match experimental data from long term tests that can be a serious limitation since we need to test many tuning parameter combinations to find the optimal match. We can thus see that solving the steady state version of this system is greatly preferable to full dynamic simulations. Essentially, the large set of nonlinear equations needs to be solved once instead of the number of time steps (thousands) considered in a dynamic simulation. Further, we note that dispersion usually plays a minor role compared to advection and reactions. By ignoring dispersion we are hence able to solve the system even more efficiently as the many unknowns in one cell can be solved as a separate system.

4.2. Simplified description

It is possible to solve the above system explicitly under simplifying, but relevant assumptions. Previous studies (Andersen and Evje 2016; Andersen and Berawala 2019; Kallesten et al. 2020) have demonstrated that injection of Ca-Mg-Na-Cl brines into chalk can be modeled assuming Ca and Mg species to substitute, by simultaneous dissolution of calcite and precipitation of magnesite to model steady state concentrations and surface ion exchange of Ca and Mg to also capture transient behavior. The mineral reaction can be stated as:

$$\mathrm{CaCO_3(s) + Mg^{2+}(aq) \leftrightarrow MgCO_3(s) + Ca^{2+}(aq)}, \tag{29}$$

This reaction implies generation of magnesite corresponds to equal amount dissolution of calcite. Let $\dot{r}$ denote the source term of magnesite generation in the reaction. It follows that:

$$\dot{r}_m = \dot{r}, \qquad \dot{r}_c = -\dot{r}, \qquad \dot{r}_{Ca} = \dot{r}, \qquad \dot{r}_{Mg} = -\dot{r}, \qquad \dot{r}_C = 0, \qquad \dot{r}_{Cl} = 0. \tag{30}$$

As Cl and C have zero source terms we do not study them further, but note that they obtain their (constant) injected concentration at steady state and can be described by the analytical solution of an advection-dispersion equation during the transient period, see for example Green and Willhite (2018). The system can be described by:

$$\partial_t C_{Ca} = -v\partial_x C_{Ca} + D\partial_{xx} C_{Ca} + \dot{r}, \tag{31}$$

$$\partial_t C_{Mg} = -v\partial_x C_{Mg} + D\partial_{xx} C_{Mg} - \dot{r}, \tag{32}$$

$$\partial_t \rho_c = -\dot{r}, \tag{33}$$

$$\partial_t \rho_m = \dot{r}. \tag{34}$$

The injected composition of reactive ions is denoted:

$$C_{Ca}(x=0) = C_{Ca}^{inj}, \qquad C_{Mg}(x=0) = C_{Mg}^{inj} \tag{35}$$

The reaction rate $\dot{r}$ is assumed to take the following form, modified from Andersen and Berawala (2019):

$$\dot{r} = k_1\left(f_{Mg} - k_2 f_{Ca}\right)^n, \qquad f_i = \frac{C_i}{C_{tot}}, \qquad C_{tot} = C_{Ca} + C_{Mg}. \tag{36}$$

f_i is the fraction of divalent ions composed by species $i = \mathrm{Ca}, \mathrm{Mg}$. $k_1\left[\left(\frac{\mathrm{mol}}{\mathrm{m}^3}\right)/\mathrm{s}\right]$ is the rate coefficient, $n\,[-]$ is the reaction order and $k_2\,[-]$ is a reaction equilibrium constant, seen as follows: By setting the reaction rate to zero $\dot{r} = 0$ we find the equilibrium concentrations C_{ca}^{eq}, C_{mg}^{eq} which are related by:

$$k_2 = C_{mg}^{eq}/C_{ca}^{eq} \tag{37}$$

In other words, the rate expression implies that at equilibrium the two species will establish a fixed concentration ratio, which is k_2. The equilibrium generally depends on the activities, but since Ca and Mg have same valence, their activity coefficients are similar for most ionic strengths (Appelo and Postma 2005), giving the same result. At high C_{mg} and low C_{ca}, magnesite will precipitate, while calcite will dissolve. The rate expression is assumed valid with constant parameters for different compositions and ionic strengths, although the parameters can change according to temperature.

4.2.1. Steady state

At steady state all the initial composition has been displaced. As the ions are substituted, we have at any point in the system:

$$C_{Ca}(x) + C_{Mg}(x) = C_{Ca}^{inj} + C_{Mg}^{inj} = C_{tot} \tag{38}$$

implying that finding the steady state solution for one concentration provides the solution for the other. It also implies that the gain in Ca (e.g., at the outlet) equals the loss in Mg:

$$C_{Ca}(x) - C_{Ca}^{inj} = C_{Mg}^{inj} - C_{Mg}(x) \tag{39}$$

For a given injected composition, the preservation of injected sum of concentrations and the zero reaction rate, determine the equilibrium composition:

$$C_{Ca}^{eq}\left(C_{Ca}^{inj}, C_{Mg}^{inj}\right) = \frac{C_{Ca}^{inj} + C_{Mg}^{inj}}{1 + k_2}, \quad C_{Mg}^{eq}\left(C_{Ca}^{inj}, C_{Mg}^{inj}\right) = \frac{k_2\left(C_{Ca}^{inj} + C_{Mg}^{inj}\right)}{1 + k_2}, \tag{40}$$

Note that the equilibrium depends on the injected composition and the parameter k_2. The rate can be expressed only with the calcium concentration as

$$\dot{r} = \frac{k_1}{C_{tot}^n}\left(C_{tot} - (1 + k_2)C_{Ca}\right)^n, \tag{41}$$

The steady state equation of Ca concentration can then be solved.

$$0 = -v\partial_x C_{Ca} + D\partial_{xx} C_{Ca} + \dot{r}, \tag{42}$$

Note that since the cells are coupled a fully implicit numerical method is required to solve this equation. Once found, the solution $C_{Ca}(x)$ provides $C_{Mg}(x)$ and $\dot{r}(x)$. By ignoring the dispersion term we can however solve the system analytically. If $n = 1$ we get exponential spatial distributions of concentration and reaction rate:

$$C_{Ca}(x) = C_{Ca}^{eq} - \left(C_{Ca}^{eq} - C_{Ca}^{inj}\right)\exp\left[-N_{Da,1}\frac{x}{L}\right], \tag{43}$$

$$C_{Mg}(x) = C_{Mg}^{eq} + \left(C_{Mg}^{inj} - C_{Mg}^{eq}\right)\exp\left[-N_{Da,1}\frac{x}{L}\right], \tag{44}$$

$$\dot{r}(x) = k_1\left(f_{Mg}^{inj} - k_2 f_{Ca}^{inj}\right)\exp\left[-N_{Da,1}\frac{x}{L}\right], \tag{45}$$

$$N_{Da,1} = (1+k_2)\frac{k_1 L}{v C_{tot}}, \qquad (n=1). \tag{46}$$

For cases with $n \neq 1$ the solution is given by:

$$C_{Ca}(x) = C_{Ca}^{eq} - \left(C_{Ca}^{eq} - C_{Ca}^{inj}\right)\left[1 + \left(\frac{C_{Ca}^{eq} - C_{Ca}^{inj}}{C_{Mg}^{inj} - k_2 C_{Ca}^{inj}}\right)^{n-1} N_{Da,n}\frac{x}{L}\right]^{\frac{1}{-n+1}}, \tag{47}$$

$$C_{Mg}(x) = C_{Mg}^{eq} + \left(C_{Mg}^{inj} - C_{Mg}^{eq}\right)\left[1 + \left(\frac{C_{Mg}^{inj} - C_{Mg}^{eq}}{C_{Mg}^{inj} - k_2 C_{Ca}^{inj}}\right)^{n-1} N_{Da,n}\frac{x}{L}\right]^{\frac{1}{-n+1}}, \tag{48}$$

$$\dot{r}(x) = k_1\left(\frac{C_{Mg}^{inj} - k_2 C_{Ca}^{inj}}{C_{Ca}^{inj} + C_{Mg}^{inj}}\right)^{n}\left[1 + \frac{1}{(1+k_2)^{n-1}} N_{Da,n}\frac{x}{L}\right]^{\frac{n}{-n+1}}, \tag{49}$$

$$N_{Da,n} = (1+k_2)^n \frac{k_1 L(n-1)}{C_{tot} v_w}\left(\frac{C_{Mg}^{inj}}{C_{tot}} - k_2\frac{C_{Ca}^{inj}}{C_{tot}}\right)^{n-1}, \qquad (n \neq 1). \tag{50}$$

In the above expressions dimensionless Damköhler numbers $N_{Da,n}$ have been applied, which express the ratio of residence time to a reaction time scale (Kee et al. 2005; Fogler 2010). For large $N_{Da,n}$ the brine interacts strongly during its residence time. In the expressions for $\dot{r}(x)$, the highest reaction rate is found at the inlet, as evaluated by the rate expression at the injected composition. The reaction rate then gradually approaches zero with distance from the inlet, and the brine concentrations approach their equilibrium values C_i^{eq}. Steady state effluent data are matched by evaluating $C_{Ca}(x = L)$ and $C_{Mg}(x = L)$ at same pore velocities and injection concentrations as the experimental data and assuming values for the reaction kinetic parameters.

5. Results and discussion

5.1. Experimental observations

A total of four tests were performed. Three tests with SK chalk where SKA1 and SKA2 were run at 130 °C, but different brine compositions: 0.0445 M in -and 0.219 M $MgCl_2$. SKA1 used the high concentration the entire experiment, while SKA2 used the high concentration during an initial shut-in period of 21 days and 14 days of injection, before continuing the rest of the experiment at low concentration injection. The third SK core SKA3 was also flooded with 0.219 M $MgCl_2$, but the test was performed at 100°C to investigate temperature effects. The Kansas chalk core KR30 was flooded with 0.219 M $MgCl_2$ at 130°C to investigate the effect of chalk type.

During a given experiment the rate was kept constant until Mg and Ca concentrations appeared to stabilize and then set to another level. In some cases, stable concentrations were not achieved when the rate was changed, but it is believed most of the change in concentration had taken place. The measured effluent concentration minus the injected concentrations of Ca and Mg are plotted against pore volumes injected for SKA1 and KR30 in **Figure 3** and **Figure 4**, respectively. The profiles appear symmetrical. Changing the injection rate results in a period where the concentrations change gradually before stabilizing to steady state. Considering the stabilized data, higher injection rate tends to give less change in

concentration from the injected values. For SKA1 there was some scatter in the concentrations at a given rate, but representative averages could be found.

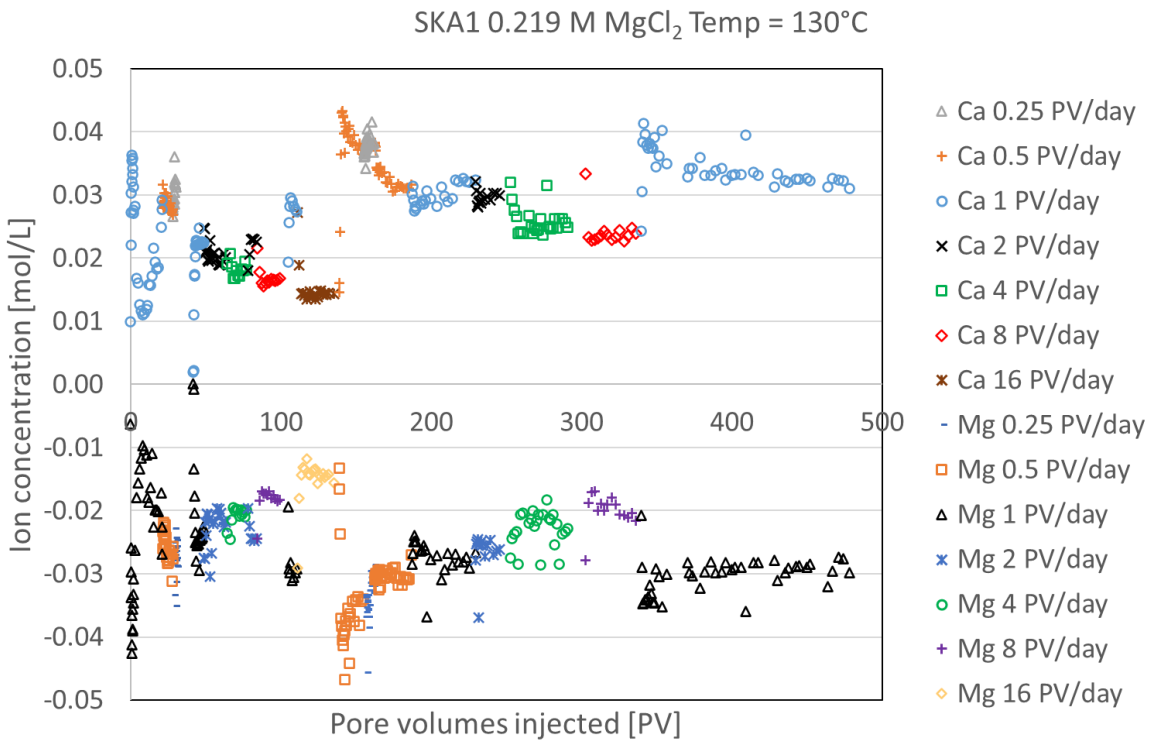

Figure 3 Measurements of Ca and Mg concentration changes (produced minus injected) against pore volumes injected for SKA1. Only the first 480 PVs of data are presented, see Table 4 for more details.

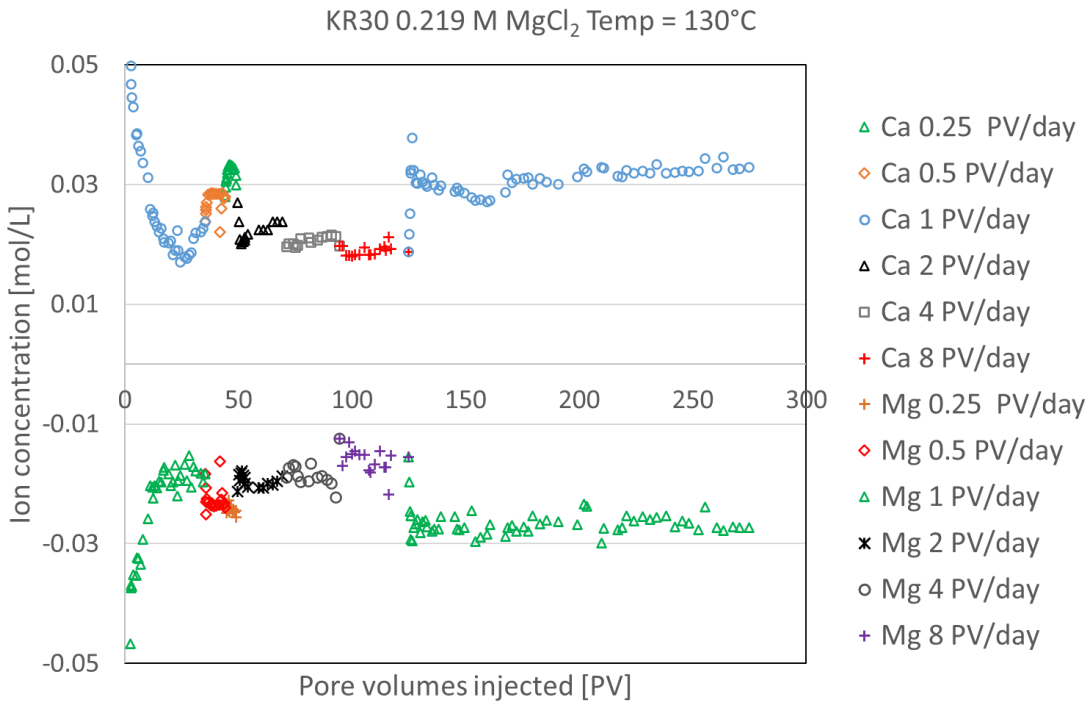

Figure 4 Measurements of Ca and Mg concentration changes (produced minus injected) against pore volumes injected

for KR30.

The shut-in data were observed to deviate from the injection data: During injection it was always observed that the effluent chloride concentration remained close to the injected concentration, similar with previous studies (Madland et al. 2011; Megawati et al. 2015). However, right after shut-in the produced chloride concentrations were significantly higher than the concentration applied when filling the core, as illustrated in **Figure 5**. Further, the flooding data in this and previous studies indicated a very similar gain of Ca and loss of Mg during $MgCl_2$ injection. The sum of Mg and Ca concentrations during shut-in increased compared to the injected sum. The increase corresponded closely with net zero charge compensating the higher Cl concentrations. The changes in Mg and Ca were unsymmetric, with more gain in Ca than loss of Mg, see **Figure 5**. Soon after the in-situ 1 PV had been displaced, the observations went back to the expected behavior. For better comparison with flooding data, the average change in divalent cation concentrations Ca and Mg during shut-in, called ΔC_{div}, was considered instead of their individual change.

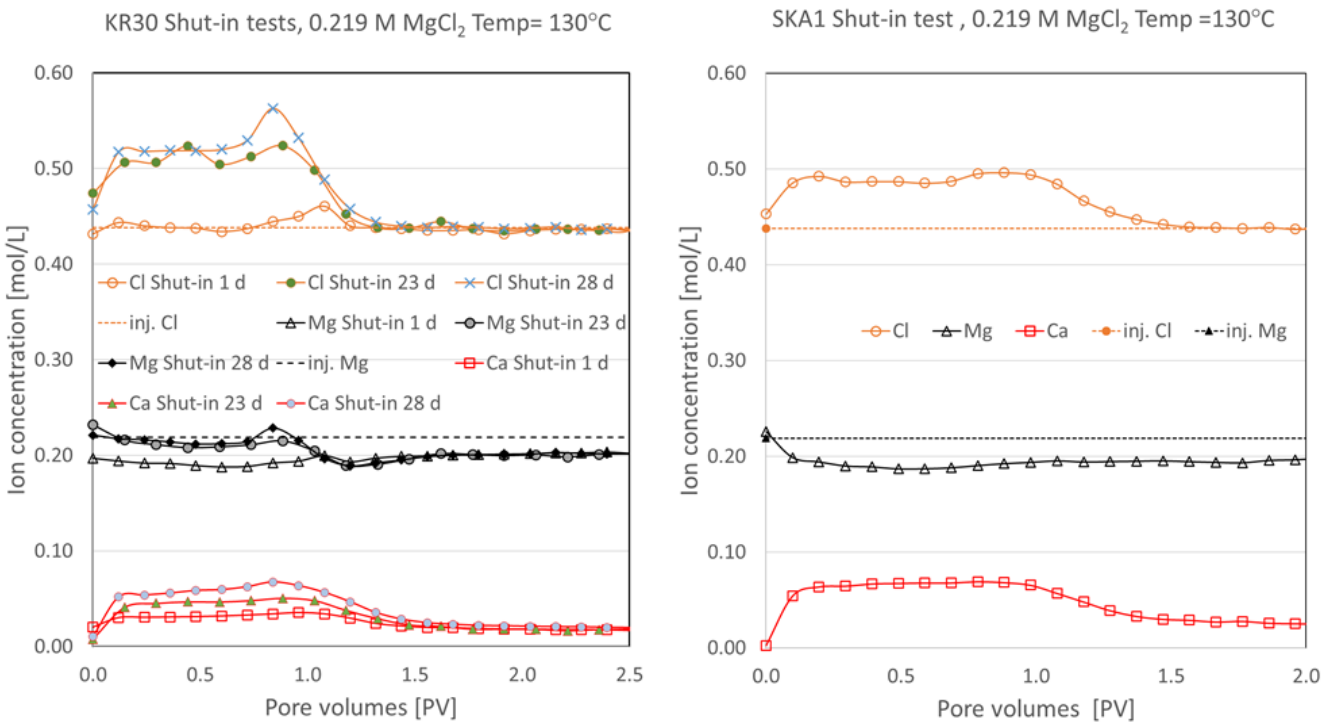

Figure 5 Effluent concentrations (pointed lines) of Ca, Mg and Cl following displacement of the pore fluid after shut-in tests in KR30 and SKA1. Dashed lines indicate initial fluid composition.

5.2. Steady state experimental data and match with analytical model

The difference in measured effluent concentrations at steady state and injected concentration are shown for Ca and Mg (as $C_{Ca}(x = L) - C_{Ca}^{inj}$ and as $C_{Mg}^{inj} - C_{Mg}(x = L)$, respectively) in **Figure 6** plotted against pore velocities v. As indicated by (39) evaluated at the outlet, the gain in Ca and loss of Mg given by these expressions are expected to be similar. The pore velocity was calculated as volumetric rate divided by porous cross section for injection data. For the shut-in data, a volumetric rate was first calculated as the pore volume divided by the residence (shut-in) time before calculating the pore velocity. All the tests were flooded in the range 0.25 to 8 PV/d except SKA1 that also was flooded at 16 PV/d. The shut-in tests gave equivalent rates as low as 1/26 – 1/28 PV/d for all the tests. The mentioned correction seemed to align

these data on the same trend as the rest, i.e. data which had lower equivalent rates generally had higher concentration changes.

The data in **Figure 6** are plotted together with the best fitted solution of the analytical model (47), (48) and (50). These solutions are explicit and do not depend on any numerical discretization or iterative procedures. The steady state measurements of the cores are also listed in **Appendix A**. SKA2 started the test with a high concentration shut-in test followed by flooding but used low concentration later for the main duration of the test. The high concentration data were comparable with the setup for SKA1 which used high concentration the entire test and they were plotted together. Especially the flooding data of the two tests overlapped well. SKA1 and SKA2 (Stevns Klint chalk and same temperature 130 °C) were matched with same reaction kinetic parameters, while SKA3 (lower temperature 100 °C) and KR30 (Kansas chalk) were tuned individually. A better match of the data from SKA2 could be obtained by matching these data separately, but combining the data we get a reaction kinetic model representative at both high and low concentrations. The parameters are listed in **Table 2** and include the reaction coefficient k_1, reaction order n and equilibrium constant k_2. Notably, k_2 indicated the level of maximum concentration change (equilibrium), k_1 shifted the curve along the velocity axis, and the reaction order n determined the slope of the curve through the data points. These features allowed a fairly unique determination of each parameter when matching the data. This is further illustrated with sensitivity analyses in the next section.

The main trend for all four tests and the model is that at higher pore velocity the change in outlet concentration (from the injected concentration) is reduced. The change goes to zero at infinite pore velocity and the concentrations go towards the equilibrium values at zero speed. The gain in Ca is similar to the loss of Mg although we can detect more gain in Ca than loss of Mg, especially for SKA2 and KR30. The tests with both high temperature and high concentration (SKA1 and KR30) give similar high concentration changes (0.01 to 0.04 mol/L), **Figure 3** and **Figure 4**. The tests injected at low temperature (SKA3) or low concentration (SKA2) observed less compositional changes (≤ 0.015 mol/L).

The data also display scatter around the main trend, quantified by the RMSE in **Table 2**. Notably, the RMSE is larger for tests where concentration change is larger (e.g. at high injected concentration and high temperature). Some variation can be due to not reaching steady state in all cases. It is also possible that changes within the core of e.g. specific surface area could alter the reactive interaction (Qin and Beckingham 2021). However, the difference in response between two tests with same rate was greater compared to the variation seen with time while keeping the same rate when steady state was established, see for example the Mg and Ca response at 1 PV/d between 125 and 275 PVs compared to the response after 35 PVs in **Figure 4**. Previous studies (Andersen et al. 2018) where $MgCl_2$ was flooded at high temperature in these chalk types demonstrated that the specific surface area can increase, but within close order of magnitude as the initial value. Andersen and Berawala (2019) calculated that porosity does not change significantly with chemical reactions in these type experiments, since the reduction in mineral volume when magnesite precipitates and calcite dissolves (8.80 mL reduction in solid volume per moles substituted) is small compared to the pore volume. When large stresses were applied chemical reactions however weakened the rock and resulted in porosity reduction by enhanced compaction.

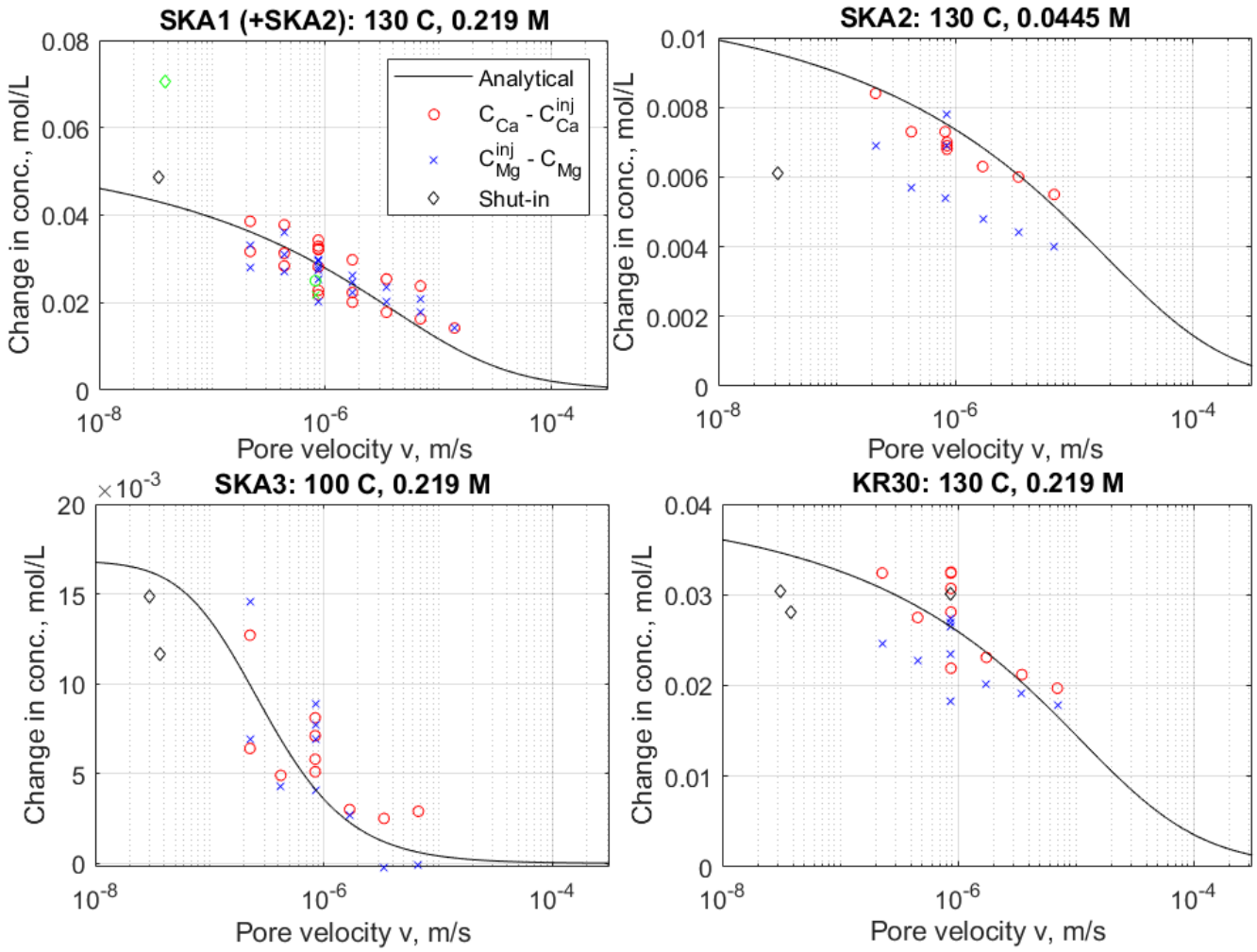

Figure 6 Measured changes in steady state outlet concentration $C_i(x = L)$ compared to the injected concentration C_i^{inj} (gain of Ca as red points and loss of Mg as blue crosses) plotted against pore velocities. Shut-in data represent the average of Ca gain and Mg loss at a given condition and the pore velocity is based on residence time and core length. Black lines represent the best fitted analytical solution (47), (48) and (50) by tuning the parameters k_1, k_2, n. The green points indicate data from SKA2 under same conditions as- and plotted with the data from SKA1.

Table 2 Reaction kinetic parameters, matching conditions and RMSE between the model and data.

Chalk type	Temperature [°C]	k_1 [mol/m3/s]	k_2 [-]	n [-]	$RMSE$ [mol/L]
Stevns Klint	130 °C	3e-3	3.0	5	0.0063 (high conc), 0.0014 (low conc)
Stevns Klint	100 °C	6e-5	12	1.5	0.0027
Kansas	130 °C	6e-3	4.5	4.5	0.0040

5.3. Sensitivity analysis: Reaction kinetic parameters

In all the following examples a 0.07 m core was assumed, where 1e-6 m/s pore velocity corresponds closely with 1 PV/d. The role of the reaction kinetic parameters is investigated in terms of how they affect the profiles of outlet concentration change vs pore velocity. As reference we assume reaction kinetics for Stevns Klint at 130 °C and injecting 0.219 M $MgCl_2$. A wide range of pore velocities was considered to include the predicted end states. In **Figure 7**, k_1 was varied 4 orders of magnitude, where the range includes the value from 100 °C.

At high pore velocity the brine does not have time to react and there is zero concentration change. At very low pore velocity the brine has enough time to reach equilibrium and the concentrations reach their maximum change. Increasing k_1 shifts the curve on the pore velocity axis. It is the Damkohler number that controls the solution so an increase of k_1 by a given factor means the pore velocity increased by the same factor will give same response. Equivalently, if the reaction goes faster, less residence time is needed to get same response.

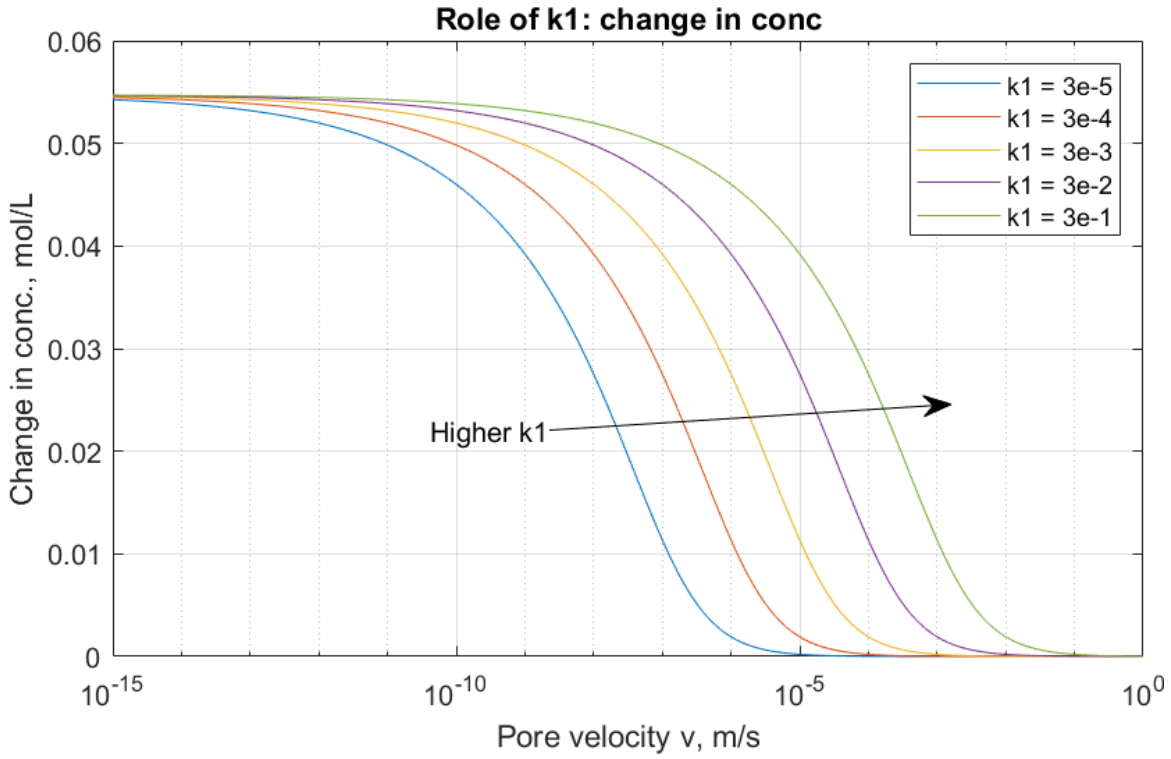

Figure 7 Simulated change in Ca/Mg outlet concentration from injected concentration (0.219 M $MgCl_2$) with pore velocity for different k1. The reaction kinetic parameters for Stevns Klint at 130 °C were used as reference (the base value of k_1 is 3e-3).

The equilibrium constant k_2 is varied in **Figure 8** from 0.3 to 30, including the matched values. Higher k_2, by definition, means there will be higher ratio of Mg to Ca at equilibrium. Since only Mg is injected with $MgCl_2$ a higher Mg/Ca ratio means less concentration change at equilibrium. As we observed concentration changes around 0.04 mol/L in the flooding experiments we should have k_2 closer to 3 than 10 to allow those changes with the model, but potentially lower than 3. The experiments did not demonstrate a very clear plateau which indicates that the reactions are relatively slow near equilibrium, even at high temperature. The trend from the flooding to shut-in data indicated that an equilibrium might be approaching. More data in the low pore velocity region would allow better prediction of k_2.

Andersen and Berawala (2019) used PHREEQC to calculate k_2 for Ca-Mg-Na-Cl brines in equilibrium with calcite where magnesite could precipitate. They predicted that k_2 was close to constant at a given temperature for a wide range of concentrations. However, the predicted $k_2 = 0.38$-0.40 (at 130 °C) was found unrealistic when matching Liege chalk flooding experiments, and a value of 4.5 was needed. In all the calculations it was found that the sum of Ca and Mg concentrations was preserved.

We also find here that the values of k_2 needed to match the data are much higher for Stevns Klint and Kansas than the predicted value of 0.39, as the concentration changes obtained with that value are far beyond observed values. It would require a very high reaction order n to explain the slope in the data and not be possible to match high and low concentration data consistently. As equilibrium was not directly

observed, the obtained k_2 and other parameter values should be considered matching parameters that fit the observed data and only estimate the true values. Better data will give better estimates. True equality between k_2 and the concentration ratio is only obtained from effluent concentrations at zero velocity (infinite residence time). We rely on trends in the data and that the scatter is sufficiently low to constrain the model parameters. By normalizing the concentration curves to their end values $\Delta C/C_{eq}$ we see that k_2 also has some effect on the location of the curve. For example, a higher pore velocity is needed at higher k_2 to reach the same fraction of the equilibrium change in concentration.

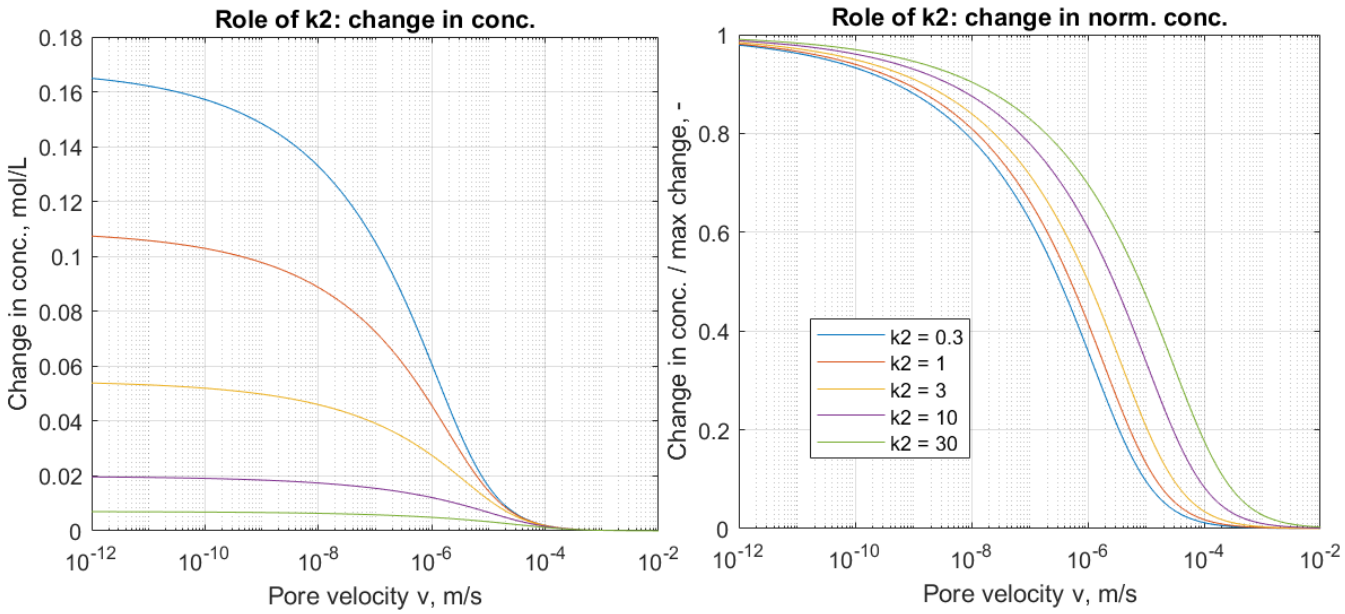

Figure 8 Simulated change in Ca/Mg outlet concentration from injected concentration (0.219 M $MgCl_2$) with pore velocity for different k2 (left). Right: Changes normalized by the equilibrium change. The reaction kinetic parameters for Stevns Klint at 130 °C were used as reference (the base value of k_2 is 3).

The reaction order n in the rate expression is varied in **Figure 9**. In all cases the outlet concentration change as function of pore velocity gives identical behavior at high enough pore velocities. That is because the Mg fraction of divalent ions approaches 1 (only Mg and no Ca is injected), such that the impact of n is insignificant. If a brine was injected with both Mg and Ca the rate would have depended on n also at high rates. At low n the brine quickly reaches the equilibrium concentration as the pore velocity is reduced. This is because the reaction rate does not reduce as fast with changes in composition. At high n the equilibrium concentration is approached only when the pore velocity is reduced by several orders of magnitude. The lowest displayed pore velocities are not expected, but they correspond to residence times that reach or exceed field time scales.

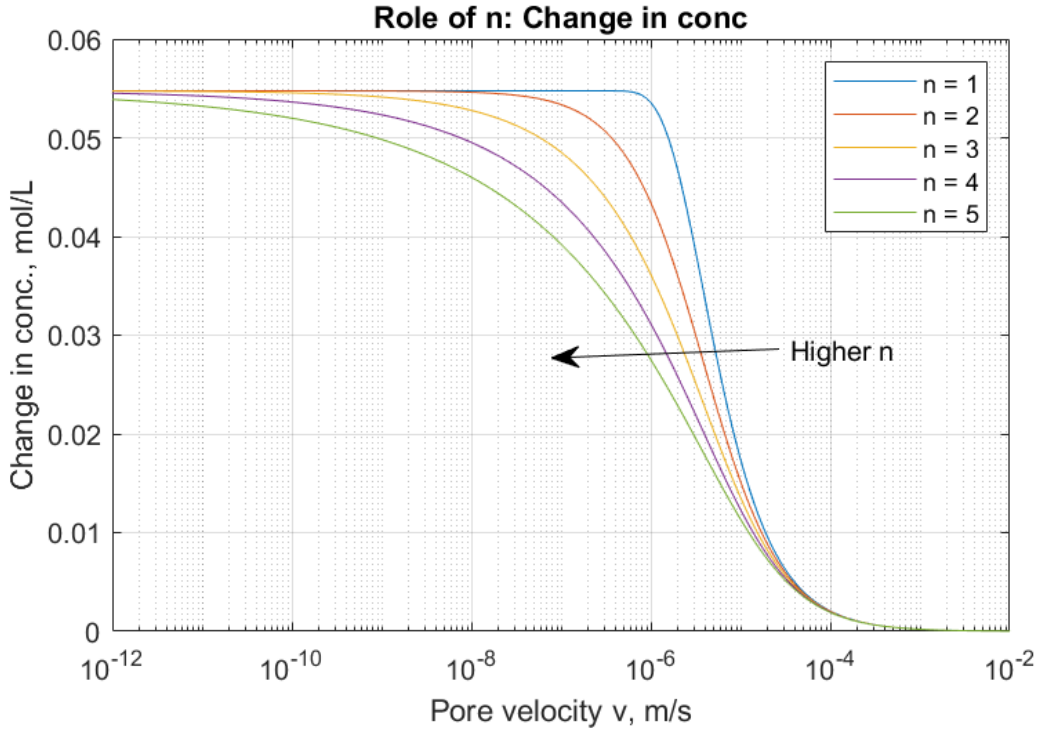

Figure 9 Simulated change in Ca/Mg outlet concentration from injected concentration (0.219 M $MgCl_2$) with pore velocity for different n. The reaction kinetic parameters for Stevns Klint at 130 °C were used as reference (the base value of n is 5).

5.4. Concentration and reaction rate spatial profiles

The spatial profiles of concentration and reaction rate are plotted for different pore velocities (from 1e-10 to 1e-4 m/s) based on the reaction kinetics determined for Stevns Klint at 130 and 100 °C, in **Figure 10** and **Figure 11**, respectively. At high injection rates the concentrations change little and linearly, explained by that the brine composition and thus reaction rate remains similar throughout the core. This provides similar gain or loss of ions at any point. As the pore velocity is reduced the brine has more time to react and most of the changes of the brine composition occur close to the inlet while the composition approaches the equilibrium composition further in. The high reaction order at 130 °C indicates that the brine loses reactivity fast with changes in composition and does not reach equilibrium even at very low pore velocities, and although compositional changes occur mainly at the inlet. Considering the relative reaction rate we see that at 1e-6 m/s (1 PV/d) there is about 30 times higher reaction rate at the inlet as at the outlet. This corresponds very well with long term experiments performed on Liege chalk at 130 °C, where the magnesium content at the inlet was 11 times higher in the first of six core slices compared to the last slice (Zimmermann et al. 2015), and especially, significant changes were observed over the entire core as we predict. A ratio close to 11 is in fact obtained by our prediction when considering averages of the outer 6th intervals rather than the end points.

In the case of 100 °C, the matched reaction order of $n = 1.5$ is much lower than at 130 °C, 5. The low n allows the reaction rate to stay high with compositional changes and means the brine can get closer to the equilibrium before the rate gets very small. As seen, the concentration profiles approach the equilibrium when reducing the rate and it is predicted that the pore velocity 1e-8 m/s or lower would yield the equilibrium composition at the outlet. At low injection rates the reaction rate can fall very fast along the core and reach negligible values. This means that most of the reactions can occur at the inlet at low pore velocities. However, we must account for that at this temperature the rate coefficient is less than at 130 °C. Considering the pore velocity 1e-6 m/s which corresponds to ~1 PV/d the reactions go slow enough that the brine does not react much during its residence time. It is predicted that at this pore velocity

the reaction rate is similar along the core, thus giving very similar mineralogical changes at the outlet as the inlet. Reducing the pore velocity by a factor of 10 to 1e-7 m/s (purple dashed curve) would give about 10 times higher rate at the inlet as at the outlet. Relatively uniform, and significant, mineralogical changes have been observed during high temperature $MgCl_2$ flooding in chalk (Andersen et al. 2018; Minde et al. 2018).

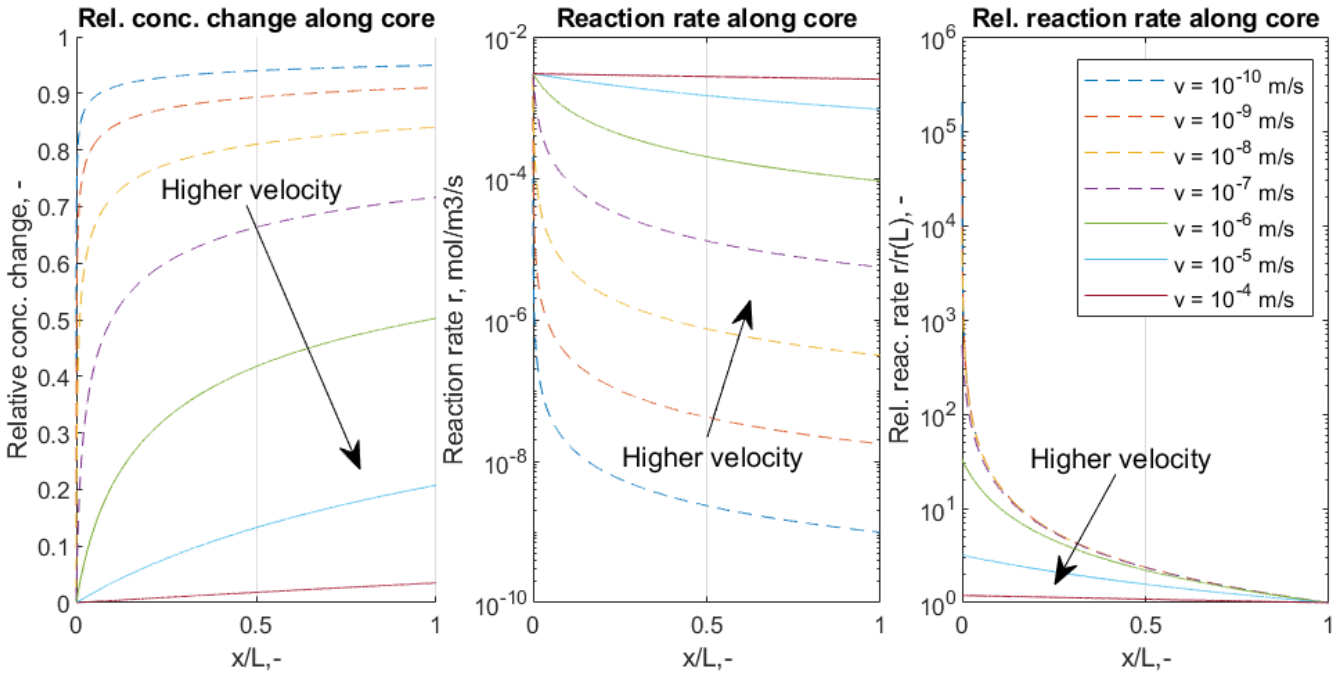

Figure 10 Simulated impact of pore velocity on spatial profiles of Ca/Mg relative concentration change (compared to maximum change), reaction rate and relative reaction rate (compared to outlet value). Stevns Klint 130 °C reaction kinetic parameters were used.

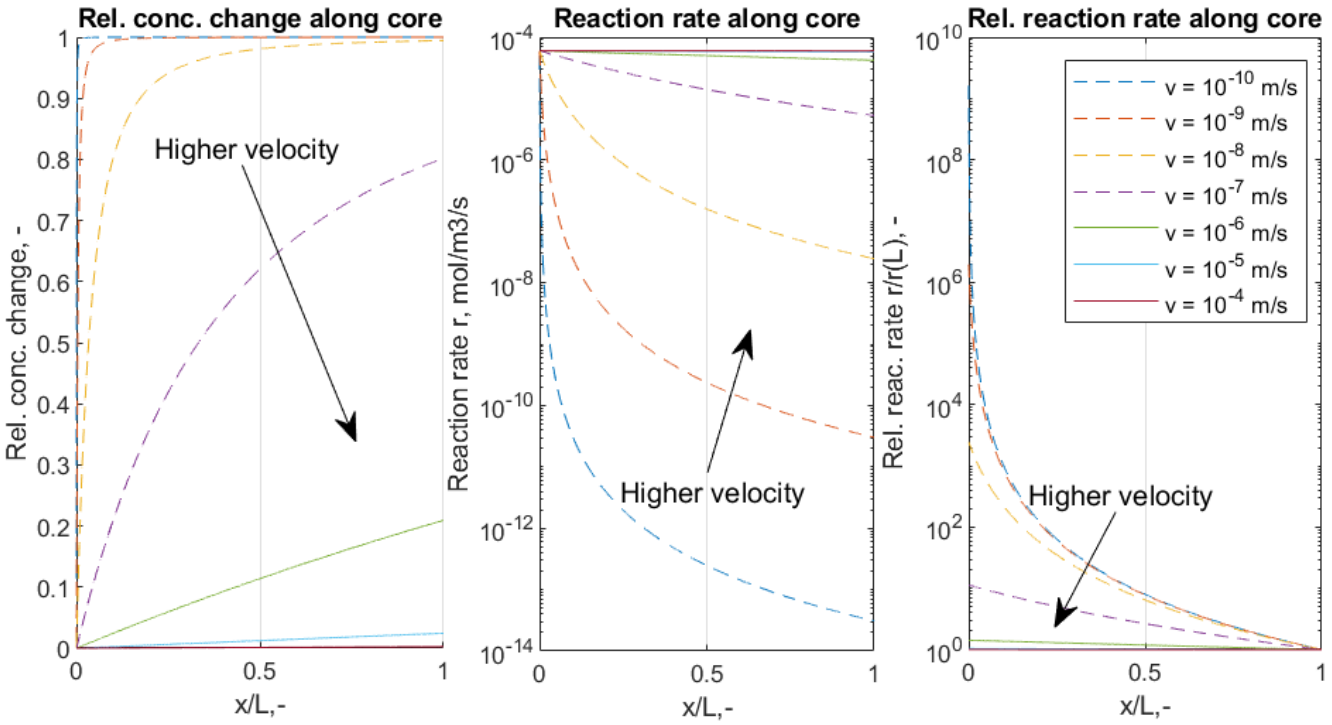

Figure 11 Simulated impact of pore velocity on spatial profiles of Ca/Mg relative concentration change (compared to maximum change), reaction rate and relative reaction rate (compared to outlet value). Stevns Klint 100 °C reaction kinetic parameters were used.

5.5. Sensitivity analysis: Dispersion

The analytical model does not account for dispersion, but it can be accounted for by numerical solution of the spatial steady state concentration profile. (10) was solved with 200 grid cells where 50 iterations were used to update the linearized equations. This was sufficient for convergence as demonstrated in **Appendix B**. The dispersion coefficient D consists of a molecular diffusion term and an advective term (Appelo and Postma 2005; Green and Willhite 2018). Assuming the advective term to be dominant we have:

$$D = \alpha v \tag{51}$$

α is called the dispersivity. Dispersion can be accounted for by only considering dispersive mixing within the porous medium or by also allowing a dispersive flux at the inlet due to the concentration gradient. The former may be more representative of core flooding experiments since the species in the injected brine is preserved and a fixed amount of pore volumes are injected per time. Both types were considered.

Dispersivity was varied assuming Stevns Klint reaction kinetics at 130 °C and injection of 0.219 M $MgCl_2$ in **Figure 12**. At higher dispersivity, less concentration change occurs at a given pore velocity. The impact of dispersion is less with zero inlet dispersive flux (dashed lines). The profile appears to shift, but preserve shape, which could impact the determination of k_1. The reaction kinetics can first be effectively estimated without dispersion and next corrected after including it. At zero dispersion the analytical solution (circles) is regained.

At high pore velocity the concentration gradient is minimal, explaining the small dispersion effect, but at low pore velocity the concentration gradient is steep from reactive compositional changes. Then dispersion acts to smooth out the concentrations, mixing reactive and less reactive brines. The high reaction order of 5 at 130 °C makes the brine sensitive to such changes. Considering the reaction kinetics at 100 °C where the order was 1.5 the impact of dispersion was much less and could be more safely ignored, see **Figure 13**. When dispersion adds a flux at the inlet (full line cases) this contributes to

maintaining the injected concentration, which is why the least concentration change is seen for these cases. More reaction would however occur inside the core since more reactive composition was supplied.

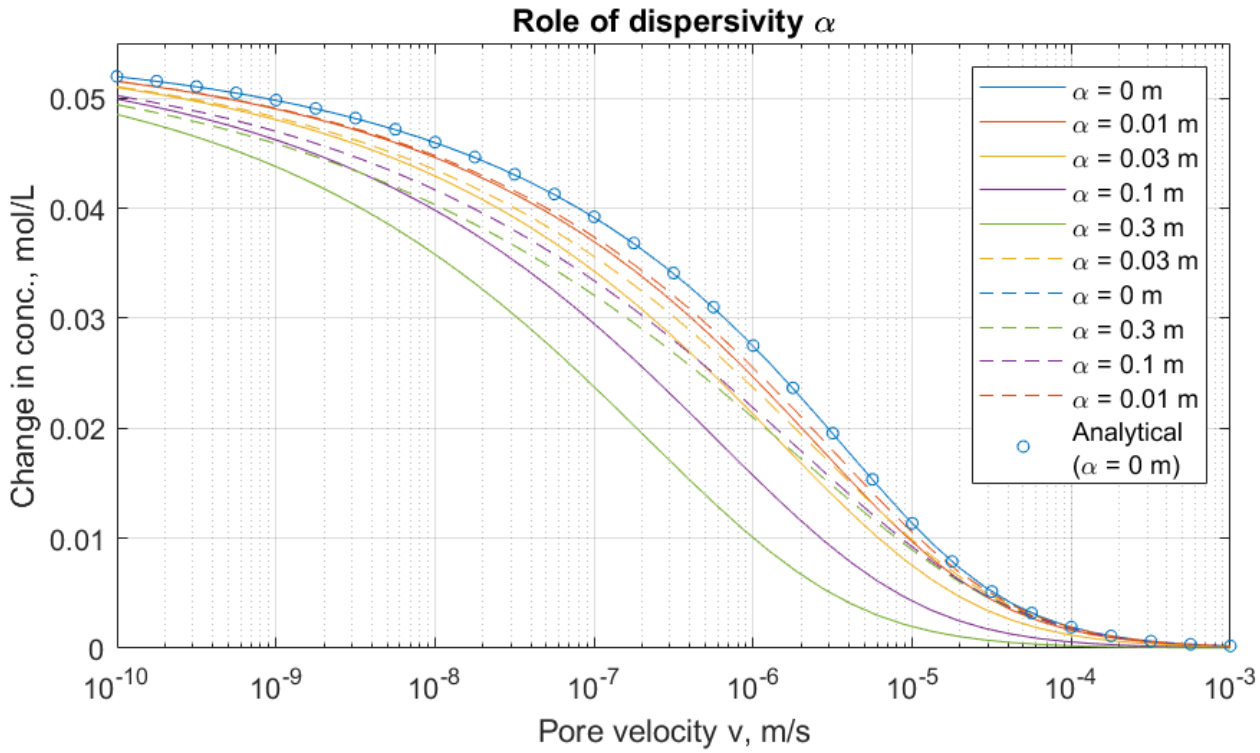

Figure 12 Simulated change in Ca/Mg outlet concentration from injected concentration (0.219 M $MgCl_2$) with pore velocity for different dispersivities α. Stevns Klint 130 °C reaction kinetic parameters were used. Dashed lines: inlet flux only based on advection. Full lines: dispersion adds a flux at the inlet. Circles: analytical solution based on zero dispersion.

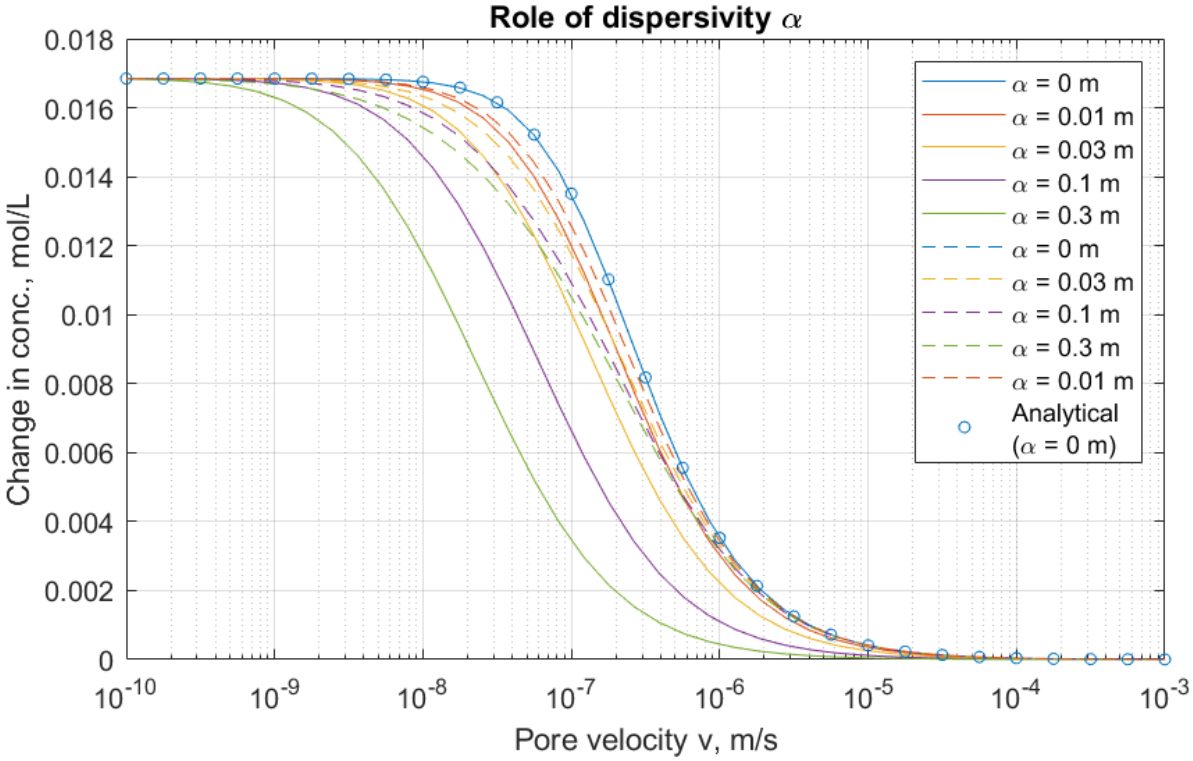

Figure 13 Simulated change in Ca/Mg outlet concentration from injected concentration (0.219 M $MgCl_2$) with pore velocity for different dispersivities α. Stevns Klint 100 °C reaction kinetic parameters were used. Dashed lines: inlet flux only based on advection. Full lines: dispersion adds a flux at the inlet. Circles: analytical solution based on zero dispersion.

5.6. Effective matching with a geochemical simulator

The geochemical simulator PHREEQC was applied to match the experimental data from SKA1, i.e. Stevns Klint chalk flooded at 130 °C with 0.219 M $MgCl_2$. The data are plotted in **Figure 14** as Ca gain and Mg loss (compared to the initial / injected values) against reaction time, set as residence time L/v_w for flooding tests and shut-in time for shut-in tests. The parameters in the calcite and magnesite reaction rates (27) were tuned to match the data. The calcite solubility constant K_c was reduced by a factor 10 as the initially predicted equilibrium of the simulator allowed far higher Ca and lower Mg concentrations than the observations indicated (the magnesite constant could also have been changed). Note that this corresponds to the difference between PHREEQCs estimated value of $k_2 = 0.39$ and the matched value ~3 with the analytical model. It is well established that solutions can be stable in non-equilibrium, including especially seawater at atmospheric conditions (Appelo and Postma 2005), which can explain why the brine does not approach the geochemically predicted equilibrium. It is also possible that the solubilities at this high temperature are not well predicted by PHREEQC. The adjustment made it much easier to tune the other parameters. In all the simulations, the predicted changes in Mg and Ca with time (green and red curves, respectively) were virtually identical, justifying the substitution assumption (29) in the simplified model. The high number of tuning parameters and the coupled nature of calcite and magnesite rates indicated that several parameter combinations could match the data in a similar way, although the data put clear constraints on the parameters. The shown match was obtained with the parameters in **Table 3**.

Table 3 Tuning parameters obtained for SKA1 when matching the reaction rates (27) with PHREEQC. It was necessary to reduce the dissolution constant of calcite by a factor 10 to match the data.

Mineral	k_i [mol/L/s]	n_i [-]
Calcite	4e-5	0.5

Magnesite	6e-8	2

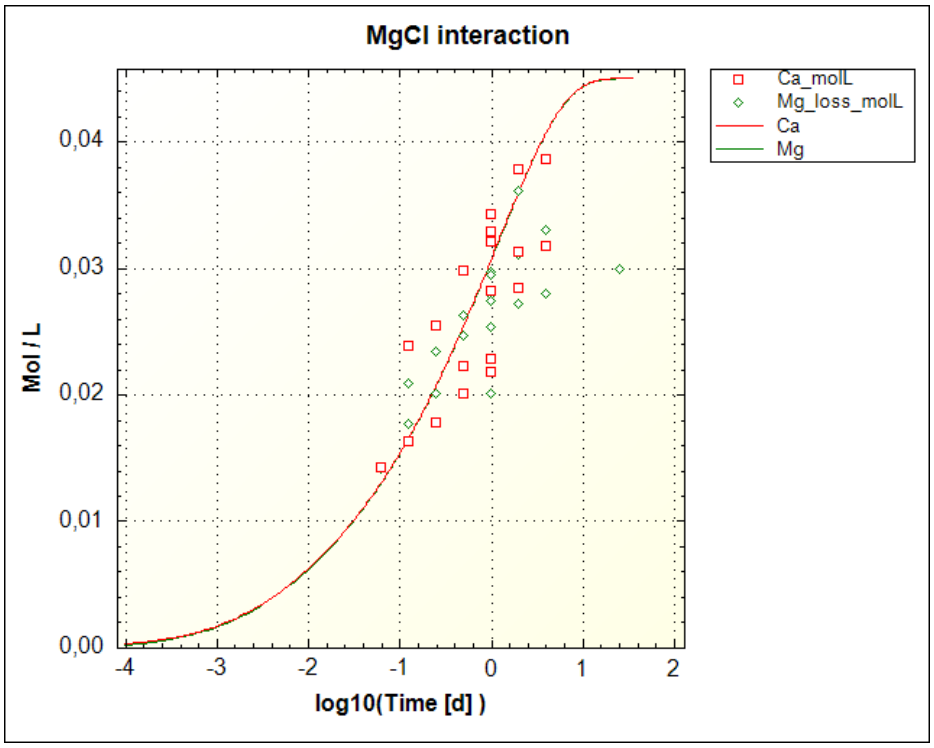

Figure 14 Experimental changes (points) in Ca and Mg concentrations from injected values for SKA1 plotted against residence time or shut-in time. Simulated responses (lines) were matched using the geochemical software PHREEQC.

5.7. Comparison with oil-saturated outcrop and reservoir chalk experiments

The experiments presented in this work were based on outcrop chalks without oil present. However, in the long run we are interested in determining and predicting reaction kinetics in reservoir chalk with the presence of crude oil and with more advanced chemistry taking place. Experiments have been performed by Sachdeva et al. (2019) on outcrop chalk from Kansas (USA) under strongly water-wet and mixed-wet conditions with oil present where 0.219 M $MgCl_2$ was flooded at 130 C at two rates. In addition, Kallesten et al. (2021a) flooded Eldfisk reservoir chalk with 0.219 M $MgCl_2$, also at 130 C, but using only one rate. The steady state measurements of gained Ca and retained Mg ($C_{Ca}(x = L) - C_{Ca}^{inj}$ and $C_{Mg}^{inj} - C_{Mg}(x = L)$, respectively) were plotted against reaction time t (the same as residence time), calculated as $t = q/(\mathrm{PV} \cdot S_w)$ where q is the injection rate, PV the pore volume and S_w the water saturation. This was compared with the values calculated by the reaction kinetics (36) for Kansas and Stevns Klint in **Figure 15**. As seen, the data overlap well with the estimated concentration changes as function of reaction time, indicating that the presence of oil did not significantly impact the reactive interactions. The scatter in the data is similar to the experiments performed in this work (Figure 6). Contrary to our experiments, there appears to be more loss of Mg than production of Ca in the experiments with oil present. It is possible that rock-water chemistry is affected by the presence of non-aqueous fluids and their composition, and furthermore the system wettability. For example, the interactions appear greater for the strongly water-wet systems than the mixed-wet system, where oil is attached to part of the surface and may limit contact with the rock.

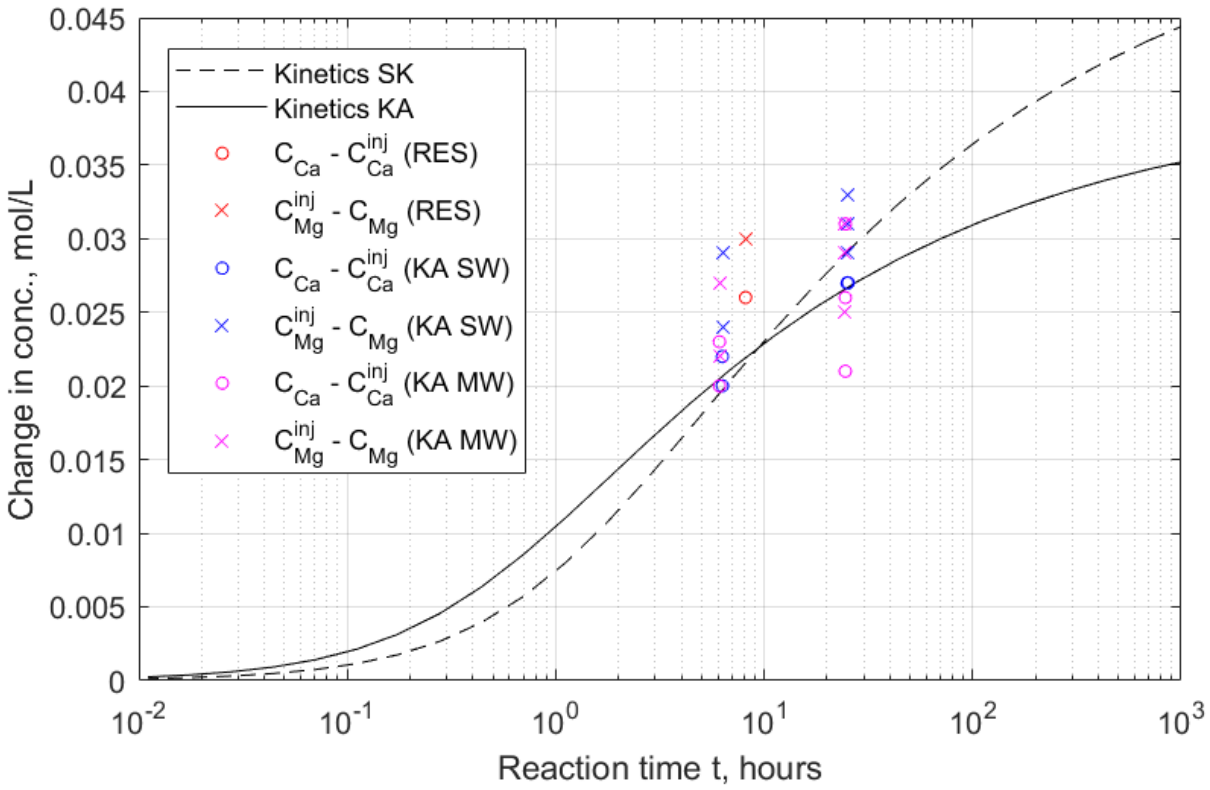

Figure 15 Comparison of predicted change in Ca and Mg concentrations for 0.219 M $MgCl_2$ in Stevns Klint (SK) and Kansas (KA) chalk at 130 C based on the determined reaction kinetics from our experiments in dashed and full lines, respectively. Also plotted are steady state changes in Ca and Mg concentrations when 0.219 M $MgCl_2$ has been flooded at 130 C in Eldfisk reservoir chalk (RES) (data from Kallesten et al. 2021a) and in strongly water-wet (SW) or mixed-wet (MW) Kansas chalk with oil present (data from Sachdeva et al. 2019).

6. Conclusions

A new way to match reaction kinetics from core flooding experiments has been proposed. By running the experiments to steady state, the data can be directly compared with modeling without running time consuming dynamical simulations in a spatially discretized system, but instead:

- Calculate the composition after the reaction time / residence time the brine has had with the system. This accounts for advection and reactions (but not dispersion). Calculation in only one cell is needed.
- Alternatively, also account for dispersion and calculate the steady state distribution through the system and report the outlet concentration. This requires solving over a grid for one state (and not multiple time steps).

Both alternatives were demonstrated on interpretation of experimental data where $MgCl_2$ was injected into Stevns Klint and Kansas chalk at high temperature (100 or 130 °C), and rates from 0.25 to 16 PV/d. The flooding experiments demonstrated non-interaction with Cl, loss of Mg and gain of Ca, which were associated with magnesite precipitation and calcite dissolution, in agreement with previous studies. The Ca gain and Mg loss were close to identical although slightly more Ca was produced than Mg lost. More chemical interaction was observed at lower injection rates in a given system.

Shut-in tests were designed to increase the reaction time as opposed to have very low injection rates. The tests gave equivalent injection rates down to 1/28 PV/d, but introduced observations different from the flooding tests: there was a gain in Cl and the gain in Ca was higher than the loss in Mg. By taking the average of Ca gain and Mg loss, the shut-in data followed the same trend as the flooding data and helped estimate the reaction equilibrium.

An analytical model based on Ca/Mg substitution and steady state between advection and reaction could model the experiments and was used to illustrate both modeling alternatives. The steady state data allowed determining the three reaction kinetic parameters accurately for each core. The determined reaction kinetics could predict reactive interactions (Ca production and Mg loss) in outcrop and reservoir chalk containing oil.

In addition, a geochemical software (PHREEQC) was used to demonstrate the first matching procedure accounting for detailed geochemical descriptions and reactions. The software predicted close to identical gain of Ca as loss of Mg with time, a substitution-like behavior also seen experimentally.

For given reaction kinetics, dispersion (with fixed dispersivity) reduces the concentration change at the outlet by (a) Mixing reactive and less reactive brine, which is more impactful if the reaction has high reaction order. This suggested that the experiments at 130 °C with reaction order 4.5-5 should be corrected for dispersivity, while the experiments at 100 °C with reaction order 1.5 did not need correction. (b) Supplying a flux of injected concentration at the inlet due to the concentration gradient. This boundary condition is less relevant for core flooding experiments as the flux is fixed. Dispersion had less impact at high pore velocity (low residence time) since the concentration gradient was low.

Acknowledgments

Andersen and Korsnes acknowledge the Research Council of Norway and the industry partners, ConocoPhillips Skandinavia AS, Aker BP ASA, Vår Energi AS, Equinor ASA, Neptune Energy Norge AS, Lundin Norway AS, Halliburton AS, Schlumberger Norge AS, and Wintershall DEA, of The National IOR Centre of Norway for support.

References

1. Amour, F., Bonto, M., Hajiabadi, M. R., & Nick, H. M. (2021, June). Sensitivity study of chemical effects on the compaction behavior of reservoir chalk (Dan field, Danish North Sea). In *55th US Rock Mechanics/Geomechanics Symposium*. OnePetro.
2. Andersen, P. Ø., Evje, S., Madland, M. V., & Hiorth, A. (2012). A geochemical model for interpretation of chalk core flooding experiments. *Chemical engineering science*, *84*, 218-241.
3. Andersen, P. Ø., & Evje, S. (2016). A model for reactive flow in fractured porous media. *Chemical Engineering Science*, *145*, 196-213.
4. Andersen, P. Ø., Wang, W., Madland, M. V., Zimmermann, U., Korsnes, R. I., Bertolino, S. R. A., ... & Gilbricht, S. (2018). Comparative study of five outcrop chalks flooded at reservoir conditions: chemo-mechanical behaviour and profiles of compositional alteration. *Transport in Porous Media*, *121*(1), 135-181.
5. Andersen, P. Ø., & Berawala, D. S. (2019). Modeling of Creep-Compacting Outcrop Chalks Injected with Ca-Mg-Na-Cl Brines at Reservoir Conditions. *SPE Journal*, *24*(06), 2889-2910.
6. Andersen, P. Ø., Walrond, K., Nainggolan, C. K., Pulido, E. Y., & Askarinezhad, R. (2020). Simulation interpretation of capillary pressure and relative permeability from laboratory waterflooding experiments in preferentially oil-wet porous media. *SPE Reservoir Evaluation & Engineering*, *23*(01), 230-246.
7. Andersen, P. Ø. (2021). Analytical modeling and correction of steady state relative permeability experiments with capillary end effects–An improved intercept method, scaling and general capillary numbers. *Oil & Gas Science and Technology–Revue d'IFP Energies nouvelles*, *76*, 61.
8. Appelo, C. A. J., & Postma, D. (2005). *Geochemistry, groundwater and pollution, 2nd ed*. Balkema Publisher, Lisse, Netherlands.
9. Berkowitz, B., Dror, I., Hansen, S. K., & Scher, H. (2016). Measurements and models of reactive transport in geological media. *Reviews of Geophysics*, *54*(4), 930-986.

10. Bonto, M., Welch, M., Lüthje, M., Andersen, S. I., Veshareh, M. J., Amour, F., ... & Nick, H. M. (2021). Challenges and enablers for large-scale CO2 storage in chalk formations. *Earth-Science Reviews*, 103826.
11. Da Gama, R. O., Lutz, B., Desjardins, P., Thompson, M., Prince, I., & Espejo, I. (2014). Integrated paleoenvironmental analysis of the Niobrara Formation: Cretaceous Western Interior Seaway, northern Colorado. *Palaeogeography, Palaeoclimatology, Palaeoecology*, *413*, 66-80.
12. Evje, S., Hiorth, A., Madland, M. V., & Korsnes, R. I. (2009). A mathematical model relevant for weakening of chalk reservoirs due to chemical reactions. *Networks & Heterogeneous Media*, *4*(4), 755.
13. Fogler, H. S. (2010). *Essentials of Chemical Reaction Engineering: Essenti Chemica Reactio Engi*. Pearson Education.
14. Green, D. W., & Willhite, G. P. (2018). *Enhanced oil recovery, 2nd ed*. Society of Petroleum Engineers, Richardson, Texas, USA.
15. Heggheim, T., Madland, M. V., Risnes, R., & Austad, T. (2005). A chemical induced enhanced weakening of chalk by seawater. *Journal of Petroleum Science and Engineering*, *46*(3), 171-184.
16. Hellmann, R., Renders, P. J., Gratier, J. P., & Guiguet, R. (2002). Experimental pressure solution compaction of chalk in aqueous solutions. Part 1. Deformation behavior and chemistry. *Water-rock interactions, ore deposits, and environmental geochemistry: A tribute to David A. Crerar*, *7*, 129-152.
17. Hjuler, M. L., & Fabricius, I. L. (2009). Engineering properties of chalk related to diagenetic variations of Upper Cretaceous onshore and offshore chalk in the North Sea area. *Journal of Petroleum Science and Engineering*, *68*(3-4), 151-170.
18. Kallesten, E., Andersen, P. Ø., Berawala, D. S., Korsnes, R. I., Madland, M. V., Omdal, E., & Zimmermann, U. (2020). Modeling of permeability and strain evolution in chemical creep compaction experiments with fractured and unfractured chalk cores conducted at reservoir conditions. *SPE Journal*, *25*(05), 2710-2728.
19. Kallesten, E. I., Cherif, Y., Madland, M. V., Korsnes, R. I., Omdal, E., Andersen, P. Ø., & Zimmermann, U. (2021a). Validation study of water weakening research from outcrop chalks performed on Eldfisk reservoir cores. *Journal of Petroleum Science and Engineering*, *198*, 108164.
20. Kallesten, E. I., Zimmermann, U., Madland, M. V., Bertolino, S., Omdal, E., & Andersen, P. Ø. (2021b). Mineralogy and geochemistry of reservoir and non-reservoir chalk from the Norwegian continental shelf. *Journal of Petroleum Science and Engineering*, *205*, 108914.
21. Kee, R. J., Coltrin, M. E., & Glarborg, P. (2005). *Chemically reacting flow: theory and practice*. John Wiley & Sons.
22. Korsnes, R. I., Madland, M. V., Austad, T., Haver, S., & Røsland, G. (2008). The effects of temperature on the water weakening of chalk by seawater. *Journal of Petroleum Science and Engineering*, *60*(3-4), 183-193.
23. Lasaga, A. C. (1998). *Kinetic theory in the earth sciences*. Princeton University Press.
24. Lebedev, M., Zhang, Y., Sarmadivaleh, M., Barifcani, A., Al-Khdheeawi, E., & Iglauer, S. (2017). Carbon geosequestration in limestone: Pore-scale dissolution and geomechanical weakening. *International Journal of Greenhouse Gas Control*, *66*, 106-119.
25. Lichtner, P. C., Steefel, C. I., & Oelkers, E. H. (Eds.). (2018). *Reactive transport in porous media* (Vol. 34). Walter de Gruyter GmbH & Co KG.
26. Madland, M. V., Hiorth, A., Omdal, E., Megawati, M., Hildebrand-Habel, T., Korsnes, R. I., ... & Cathles, L. M. (2011). Chemical alterations induced by rock–fluid interactions when injecting brines in high porosity chalks. *Transport in porous media*, *87*(3), 679-702.
27. Maury, V., Piau, J. M., & Halle, G. (1996, October). Subsidence induced by water injection in water sensitive reservoir rocks: the example of Ekofisk. In *European Petroleum Conference*. OnePetro.
28. Megawati, M., Andersen, P. Ø., Korsnes, R. I., Evje, S., Hiorth, A., & Madland, M. V. (2011). The Effect of Aqueous Chemistry pH on the Time-Dependent Deformation Behaviour of Chalk-Experimental and Modelling Study. *Pore2Fluid IFP Energies nouvelles Paris, Nov*, 16-18.

29. Megawati, M., Hiorth, A., & Madland, M. V. (2013). The impact of surface charge on the mechanical behavior of high-porosity chalk. *Rock mechanics and rock engineering*, *46*(5), 1073-1090.
30. Minde, M. W., Wang, W., Madland, M. V., Zimmermann, U., Korsnes, R. I., Bertolino, S. R., & Andersen, P. Ø. (2018). Temperature effects on rock engineering properties and rock-fluid chemistry in opal-CT-bearing chalk. *Journal of Petroleum Science and Engineering*, *169*, 454-470.
31. Morse, J. W., & Arvidson, R. S. (2002). The dissolution kinetics of major sedimentary carbonate minerals. *Earth-Science Reviews*, *58*(1-2), 51-84.
32. Parkhurst, D. L., & Appelo, C. A. J. (1999). User's guide to PHREEQC (Version 2): A computer program for speciation, batch-reaction, one-dimensional transport, and inverse geochemical calculations. *Water-resources investigations report*, *99*(4259), 312.
33. Puntervold, T., & Austad, T. (2008). Injection of seawater and mixtures with produced water into North Sea chalk formation: impact of fluid–rock interactions on wettability and scale formation. *Journal of Petroleum Science and Engineering*, *63*(1-4), 23-33.
34. Qin, F., & Beckingham, L. E. (2021). The impact of mineral reactive surface area variation on simulated mineral reactions and reaction rates. *Applied Geochemistry*, *124*, 104852.
35. Sabo, M. S., & Beckingham, L. E. (2021). Porosity-Permeability Evolution During Simultaneous Mineral Dissolution and Precipitation. *Water Resources Research*, *57*(6), e2020WR029072.
36. Sachdeva, J. S., Nermoen, A., Korsnes, R. I., & Madland, M. V. (2019). Impact of initial wettability and injection brine chemistry on mechanical behaviour of kansas chalk. *Transport in Porous Media*, *128*(2), 755-795.
37. Steefel, C. I., & MacQuarrie, K. T. (2018). *Approaches to modeling of reactive transport in porous media* (pp. 83-130). De Gruyter.
38. Surlyk, F., Damholt, T. & Bjerager, M. (2006). Stevns Klint, Denmark: Uppermost Maastrichtian chalk, Cretaceous–Tertiary boundary, and lower Danian bryozoan mound complex. *Bulletin of the Geological Society of Denmark*, *54*, 1-48.
39. Sylte, J. E., Thomas, L. K., Rhett, D. W., Bruning, D. D., & Nagel, N. B. (1999, October). Water induced compaction in the Ekofisk field. In *SPE Annual Technical Conference and Exhibition*. OnePetro.
40. Virnovsky, G. A., Guo, Y. & Skjæveland, S. M. (1995, May). Relative permeability and capillary pressure concurrently determined from steady-state flow experiments. In *IOR 1995-8th European Symposium on Improved Oil Recovery* (pp. cp-107). European Association of Geoscientists & Engineers.
41. Zimmermann, U., Madland, M. V., Nermoen, A., Hildebrand-Habel, T., Bertolino, S. A., Hiorth, A., ... & Grysan, P. (2015). Evaluation of the compositional changes during flooding of reactive fluids using scanning electron microscopy, nano-secondary ion mass spectrometry, x-ray diffraction, and whole-rock geochemistry. *AAPG Bulletin*, *99*(5), 791-805.
42. Zhang, P., Tweheyo, M. T., Austad T. (2006). Wettability alteration and improved oil recovery by spontaneous imbibition of seawater into chalk: Impact of the potential determining ions Ca2+, Mg2+, and SO42-. *Colloids and Surfaces A: Physicochem. Eng. Aspects*, *301*, 199–208.

Nomenclature

Roman

a_i	=	Activity
$\tilde{a}_i, \tilde{b}_i$	=	Ion specific activity coefficient parameters, -
A, B	=	Temperature dependent activity coefficient parameters, -
C_i	=	Brine concentration of species i, mol / m^3
D	=	Dispersion coefficient, m^2 / s
f_i	=	Fraction of divalent ions consisting of species i, -

I_0	=	Ionic strength, -
K	=	Equilibrium constant, -
k_1	=	Reaction rate constant, $\left(\frac{\text{mol}}{\text{m}^3}\right)/\text{s}$
k_2	=	Reaction rate equilibrium constant, -
k_j	=	Mineral reaction rate constant, $\left(\frac{\text{mol}}{\text{m}^3}\right)/\text{s}$
L	=	Core length, m
m_i	=	Free ion concentration of species i, mol/m3
n	=	Reaction order, -
$n_{i,i'}$	=	Concentration of complex between ion species i and i', mol/m3
$N_{Da,n}$	=	Dahmköhler number for reaction order n, -
N_{ions}	=	Number of aqueous ions, -
N_{it}	=	Number of iterations, -
N_{min}	=	Number of minerals, -
N_x	=	Number of grid cells, -
$\dot{r}_i, \dot{r}_j$	=	Source term of species i or j from reactions, mol / m^3 / s
$\dot{r}$	=	Net reaction rate for magnesite precipitation and calcite dissolution, mol / m^3 / s
T	=	Absolute temperature, K
v	=	Brine pore velocity, m/s
x	=	Distance from inlet, m
X	=	Scaled distance from inlet, -
z_i	=	Ionic valence, -

Greek

α	=	Dispersivity, m
γ_i	=	Activity coefficient, -
ρ_j	=	Mineral concentration, mol / m^3
ρ_i^s	=	Surface species concentration, mol / m^3
τ	=	Shut-in time period, s
ϕ	=	Porosity, -
Ω_j	=	Saturation state of mineral j, -

Indices

aq	=	Aqueous
c	=	Calcite
C	=	Carbon
Ca	=	Calcium
Cl	=	Cloride
eq	=	Equilibrium state
i	=	Aqueous species
$init$	=	Initial state
inj	=	Injected concentration state
j	=	Mineral species
k	=	Grid index
m	=	Magnesite
Mg	=	Magnesium

Abbreviations

PV	=	Pore volume
RMSE	=	Root mean square error

Appendix A: Steady state measurements

Table 4 Flow rate, injection times and measured ion concentrations for SKA1, performed at 130 °C in Stevns Klint chalk with 0.219 M $MgCl_2$. * Had not reached steady state. ^ Equivalent rate based on residence time.

Flow rate [mL/min]	Flow rate [PV/d]	Injection time [d]	Ca [mol/L]	Mg [mol/L]	Ca + Mg [mol/L]
0.028 *	1.0	0-21	0.0218	0.1989	0.2207
0.014	0.5	21-34	0.0284	0.1918	0.2202
0.007	0.25	34-88	0.0317	0.1910	0.2227
0.028	1.0	88-95	0.0228	0.1937	0.2165
0.056	2.0	95-103	0.0201	0.1967	0.2168
0.112	4.0	103-106	0.0178	0.1989	0.2167
0.056 *	2.0	106-109	0.0223	0.1944	0.2167
0.224	8.0	109-112	0.0163	0.2013	0.2176
0.028 *	1.0	112-118	0.0282	0.1893	0.2175
0.448	16.0	118-120	0.0142	0.2049	0.2191
0.014	0.5	120-152	0.0378	0.1829	0.2207
0.007	0.25	152-180	0.0386	0.1860	0.2246
0.014	0.5	180-228	0.0313	0.1880	0.2193
0.028	1.0	228-271	0.0323	0.1911	0.2234
0.056	2.0	271-281	0.0298	0.1928	0.2226
0.112	4.0	284-295	0.0254	0.1956	0.2210
0.028	1.0	295-305	0.0329	0.1893	0.2222
0.224	8.0	305-309	0.0238	0.1981	0.2219
0.028	1.0	309-546	0.0331	0.1895	0.2226
Shut-in (26 Days) 0.0011 ^	1/26 ^	547-573	0.0674	0.1891	0.2565
0.028	1.0	573-602	0.0343	0.1895	0.2238

Table 5 Flow rate, injection times and measured ion concentrations for SKA2, performed at 130 °C in Stevns Klint chalk. The test started with a shut-in phase lasting 21 days with 0.219 M $MgCl_2$ as pore fluid and a following period with flooding of 0.219 M $MgCl_2$. Next, injection of 0.0445 M $MgCl_2$ was initiated. ^ Equivalent rate based on residence time.

Flow rate [mL/min]	Flow rate [PV/d]	Injection time [d]	Ca [mol/L]	Mg [mol/L]	Ca + Mg [mol/L]
Shut-in (21 days) 0.0013 ^ (0.219 M $MgCl_2$)	1/21 ^	0-21	0.0984	0.1763	0.2748
0.027 (0.219 M $MgCl_2$)	1	33-35	0.0250	0.1974	0.2224
0.027	1.0	59-80	0.0073	0.0391	0.0463
0.014	0.52	80-123	0.0073	0.0388	0.0461
0.007	0.26	123-171	0.0084	0.0376	0.0459
0.028	1.04	171-194	0.0069	0.0376	0.0445
0.056	2.07	194-206	0.0063	0.0397	0.0460
0.112	4.15	206-221	0.0060	0.0401	0.0462
0.224	8.3	221-227	0.0055	0.0405	0.0460
0.028	1.04	227-448	0.0068	0.0376	0.0444
Shut-in (26 days) 0.0010 ^	1/26 ^	448-474	0.0138	0.0461	0.0598
0.028	1.04	474-570	0.0070	0.0367	0.0437

Table 6 Flow rate, injection times and measured ion concentrations for SKA3, performed at 100°C on Stevns Klint chalk with 0.219 M $MgCl_2$. ^ Equivalent rate based on residence time.

Flow rate [mL/min]	Flow rate [PV/d]	Injection time [d]	Ca [mol/L]	Mg [mol/L]	Ca + Mg [mol/L]
0.026	1.0	0-36	0.0051	0.2149	0.2200
0.013	0.5	36-57	0.0049	0.2147	0.2197
0.007	0.27	57-76	0.0064	0.2121	0.2185
0.052	2.0	76-85	0.0030	0.2163	0.2193
0.104	4.0	85-91	0.0025	0.2192	0.2217
0.208	8.0	91-94	0.0029	0.2191	0.2221
0.026	1.0	94-132	0.0058	0.2113	0.2171
Shut-in (23 Days) 0.0011 ^	1/23 ^	132-155	0.0130	0.2087	0.2217
0.026	1.0	155-191	0.0071	0.2121	0.2193
Shut-in (28 Days) 0.00093 ^	1/28 ^	191-219	0.0203	0.2096	0.2299
0.026	1.0	219-279	0.0081	0.2101	0.2181
0.007	0.27	279-306	0.0127	0.2044	0.2171

Table 7 Flow rate, injection times and measured ion concentrations for KR30, performed at 130 °C in Kansas chalk with 0.219 M $MgCl_2$. * Had not reached steady state. ^ Equivalent rate based on residence time.

Flow rate [mL/min]	Flow rate [PV/d]	Injection time [d]	Ca [mol/L]	Mg [mol/L]	Ca + Mg [mol/L]
0.023 *	1.0	0-35	0.0219	0.2008	0.2227
0.012	0.52	35-51	0.0275	0.1963	0.2238
0.006	0.26	51-70	0.0324	0.1944	0.2269
0.046	2.0	70-80	0.0231	0.1989	0.2220
0.092	4.0	80-86	0.0212	0.1998	0.2210
0.184	8.0	86-90	0.0197	0.2011	0.2209
0.023	1.0	90-125	0.0281	0.1917	0.2197
Shut-in (23 days) 0.0010 ^	1/23 ^	125-148	0.0481	0.2108	0.2588
0.023	1.0	148-174	0.0307	0.1921	0.2229
Shut-in (1.0 days) 0.023 ^	1/1 ^	175-176	0.0319	0.1906	0.2225
0.023	1.0	176-184	0.0324	0.1955	0.2279
Shut-in (28 days) 0.00082 ^	1/28 ^	184-212	0.0559	0.2142	0.2701
0.023	1.0	212-279	0.0325	0.1925	0.2250

Appendix B: Numerical sensitivity analysis

We demonstrate the sensitivity of the numerical solution of (10) to variation in grid discretization and number of iterations to update the concentrations in a grid cell. We consider the reaction kinetics of Stevns Klint at both 130 C and 100 C and model the concentration change against pore velocity with 0.219 M $MgCl_2$ injected. As reference the number of grid cells was $N_x = 200$ and the number of iterations to solve the linearized equations was $N_{it} = 50$. The dispersivity was $\alpha = 0.1$ m and dispersion was included at the inlet boundary. As seen in **Figure 16** the results are indistinguishable between 20 and 200 cells, while a too low number of iterations (much lower than we selected) can underestimate strong reactive interactions.

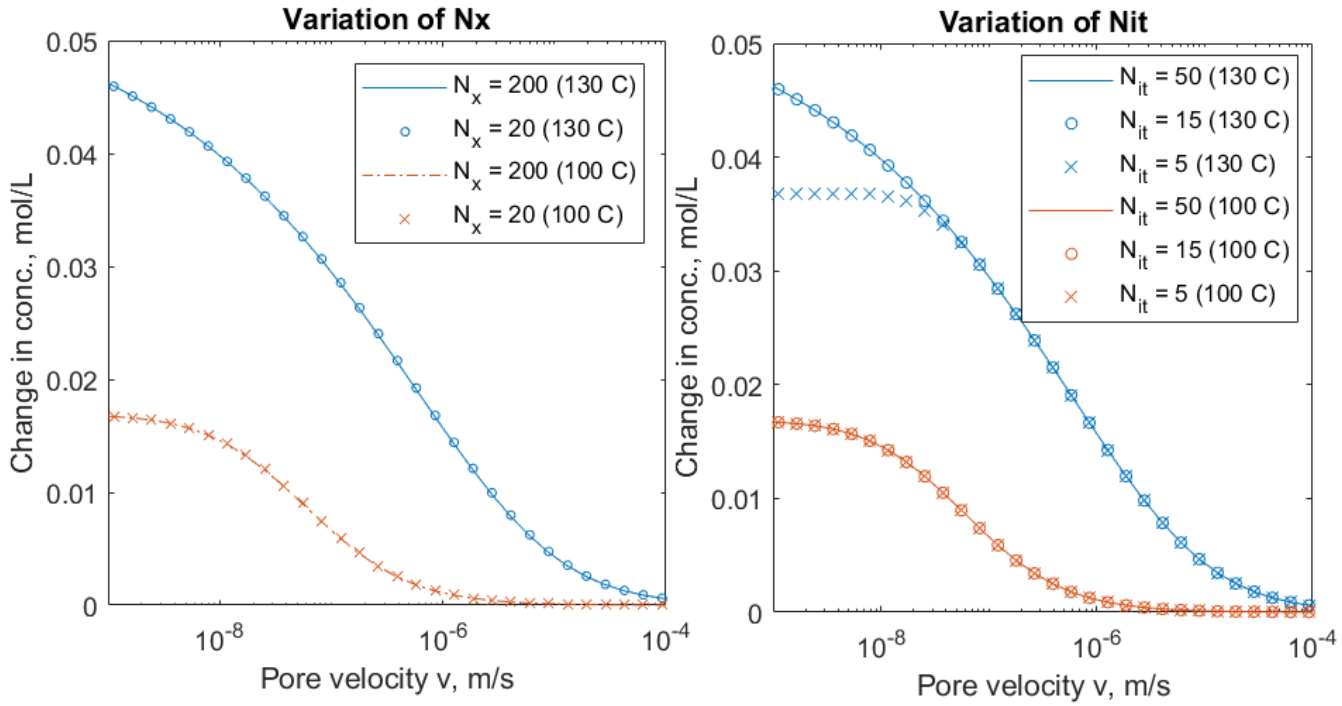

Figure 16 Sensitivity analysis of the numerical solution to the number of grid cells N_x and iterations N_{it}.